

Interim Progress Report No.1

**Electrochemical Processes for In-situ Treatment of  
Contaminated Soils**

Submitted to  
Department of Energy

by:

C.P. Huang (Principal Investigator)  
Daniel Cha (Co-Investigator)  
Jih-Hsing Chang (Graduate Research Assistant)  
Zhimin Qiang (Graduate Research Assistant)  
Menghau Sung (Graduate Research Assistant)  
Louis Cheng (Graduate Research Assistant)

Department of Civil and Environmental Engineering  
University of Delaware  
Newark, Delaware 19716

September 1996 to May 1997

# Table of Contents

<b>I. SUMMARY</b> .....	1
I. 1. Soils Characterization .....	1
1.2. Adsorption of Selected Organic Compounds on Soils .....	1
1.3. Electra-Osmosis Experiments .....	2
1.4. Electra-Fenton Experiments .....	3
<b>II. SOIL CHARACTERIZATION</b> .....	4
II. 1. Composition Analysis .....	4
11.2. Soil pH .....	4
11.3. Soil Organic Matter .....	4
11.4. Soil Effective Cation Exchange Capacity .....	4
11.5. Moisture Content .....	5
11.6. Specific Surface Area .....	5
11.7. $pH_{ZPC}$ .....	5
11.8. Hydraulic Conductivity and Hydraulic Permeability .....	5
11.9. Analysis of Organic Compounds in Soils .....	6
II. 10. Analysis of Heavy Metals in Soils .....	6
<b>III. ADSORPTION OF SELECTED ORGANIC COMPOUNDS ON SOILS</b> .....	17
III. 1. Experimental Methods .....	17
111.2. Experimental Results .....	17
<b>IV. ELECTRO-OSMOSIS EXPERIMENTS</b> .....	22
IV. 1. Experimental Methods .....	22
IV.2. Experimental Results .....	24
IV.2.1. Electra-Osmosis Water Flow .....	24
IV.2.2. Coefficient of Electra-Osmosis Permeability ( $k_e$ ) .....	25
IV.2.3. Influent-Effluent pH Changes .....	25

IV.2.4. Contaminant Removal.....	26
IV.2.5. The pH Profile, Water Content and Contaminant Distribution .....	26
IV.2.6. Mass Balance.....	27
<b>V. ELECTRO-FENTON EXPERIMENTS.....</b>	<b>42</b>
V. 1. Experimental Methods .....	42
V. 1.1. Reactor Configuration .....	42
V. 1.2. Power Supply and Equipment Configuration.....	43
V.1.3. Methods.....	44
V.2. Experimental Results .....	46
V.2.1. Effect of Current Intensity.....	46
V.2.2. Effect of Solution pH.....	46
V.2.3. Effect of Oxygen Bubbling System.....	47
V.2.4. Effect of Solution Temperature.....	47
V.2.5. Effect of Cathode Geometry.....	47
V.2.6. Current Efficiency for Hydrogen Peroxide.....	47
V.2.7. Hydrogen Peroxide Stability .....	49
<b>VI. FUTURE WORK .....</b>	<b>68</b>
VI. 1. Adsorption of Selected Organic Compounds on Soils.....	68
VI.2. Electra-Osmosis Experiments.....	68
VI.3. Electra-Fenton Experiments.....	68
<b>VII. REFERENCES .....</b>	<b>69</b>
<b>VIII. APPENDIX.....</b>	<b>71</b>
A. Soils Characterization.....	71
B. Electra-Osmosis Experiments.....	77
C. Electra-Fenton Experiments.....	78

# I. SUMMARY

## I.1. Soil Characterization

soil samples from three industrial sites at two depth ranges (2'~4' feet and 8'~ 14' feet ) were received and pertinent physico-chemical properties, such as pH, specific surface area, moisture content, organic matter content, hydraulic conductivity, cation exchange capacity (CEC), pH at zero point of charge ( $\text{pH}_{\text{zpc}}$ ), particle size distribution, organic contaminants and heavy metals fractionation were analyzed.

Results show that clay and silt are the major components in the soil samples, which exhibits a relatively low hydraulic conductivity of about  $10^{-7}$ ~ $10^{-8}$  cm/sec. The pH value of soil samples is in the neutral range (from pH 6.1 to 7.6) and its variation with depth is insignificant. Organic matter content is another important factor which affects soil properties such as specific surface area, chemical adsorption capacity and cation exchange capacity. Results indicate that the organic matter content ranges between 0.79% and 1.81%. The effective cation exchange capacity is from 13.8 to 21.2 meq/100g. The values of moisture content, specific surface area and  $\text{pH}_{\text{zpc}}$  range from 10.2~16.9 (%), 0.4~0.9 ( $\text{m}^2/\text{g}$ ) and 2.18~2.60, respectively.

## I.2. Adsorption of Selected Organic Compounds on Soils

Knowledge of the interaction of organic compounds with soil materials is important in the assessment of the mobility and fate of these compounds in the environment. The study of organic compounds adsorption on soils will provide valuable information on their potential of migration into the groundwater. In this study we investigated the adsorption of chlorophenols on kaolinite in order to obtain a general information about organics adsorption.

Chlorinated phenols are a class of priority pollutants recognized as a hazard to health and the environment, and kaolinite is a 1:1 dioctahedral clay mineral with low activity and high electroosmotic water transport efficiency. The information obtained from this adsorption experiment are useful for the understanding of organic matter adsorption on soils as well as for the electro-osmosis experiments.

Batch adsorption experiments were conducted at various soil to solution (weight) ratios (1:3 to 1:20) and at various initial concentrations of chlorophenols. Adsorption isotherms can be fitted by the Langmuir equation. Constants for the series of chlorophenols obtained from non-linear

least square are obtained (Table 3.1). The maximum adsorption density values are approximately the same for different chlorophenols indicating a common mode of binding. In order to test whether the binding of chlorophenols is occurring through equilibration of the surface and the protonated form, the pH dependence of binding was determined for 3 representative chlorophenols with different amounts of chlorine substitution. Results indicate that the data are consistent with binding of the protonated species.

### **I.3. Electra-Osmosis Experiments**

Electrochemistry plays an important role during an electro-osmosis process. The generation of pH gradients and possible effects, such as ion exchange and the change in the soil composition caused by the acid front which is originated at the anode, ensure a diminishing of the water flow compromising the efficiency of the process. The build up of acidic condition at the anode during the application of electro-osmosis process is due to the oxidation of water. The products of the oxidation are oxygen gas ( $O_2$ ) and hydrogen ions ( $H^+$ ). Inversely, the basic condition at the cathode is attributed to the reduction of water. This electrochemical reaction decomposes the water producing hydrogen gas ( $H_2$ ) and hydroxyl ions ( $OH^-$ ).

As an inovative contaminant removal method, the technique demonstrates to be effective depending upon conditions related to the physico-chemical properties of the packed soil core. Among these conditions, the pore volume was proved to be important and closely related to the removal efficiency.

In this study, the phenol distribution obtained in the soil core indicates that the contaminant movement is not uniform throughout the medium and accumulates near the cathode. This could be used as a tool to concentrate the pollutants in a specific area between the electrodes for further remediation treatment.

A 93% removal was achieved for the 2-chlorophenol showing that electroosmosis can be an effective way to remediate phenol-contaminated soils.

This work illustrates some of the practical difficulties and advantages of electro-osmosis as a clean up technique. Major considerations to the successful application of electro-osmosis include detailed physico-chemical characteristics of the contaminated soil and the electrochemistry which accompanies the electrokinetic process.

## **I.4. Electro-Fenton Experiments**

Advanced chemical oxidation processes can be applied in a very effective way for water and groundwater remediation. While most of the aqueous effluents have been treated by biological processes in the past, chemical oxidative degradation is being used for those wastes which can not be easily decomposed by biological activities. In contrast with many remediation techniques that simply transfer the waste from one part of the environment to another, oxidation processes may offer a better solution for partial or even complete degradation of the contaminants.

Hydroxyl radicals, with the second highest oxidation potential, have gained attention over the past years (Matsue et al, 1981; Sudoh et al, 1985; Huang et al, 1991). One of the most feasible systems for hydroxyl radicals generation is the electrogenerated Fenton's reagent. Hydrogen peroxide is produced in-situ in an electrochemical cell. In the presence of ferrous ions, hydrogen peroxide decomposes to hydroxyl radicals while the iron is oxidized to ferric ions.

So far, the objective of this study is to clarify the effect of various parameters on the production of hydrogen peroxide. Influential parameters, such as cell voltage and current intensity, solution pH, oxygen bubble size and oxygen quality, solution temperature, and cathode geometry were tested to determine the best working conditions which enhance the production of hydrogen peroxide. Results show that the optimum conditions are 1 Amp of current intensity, solution pH 3.0, stone diffusion system, pure oxygen, ambient solution temperature (25 °C), long finger cathode. In addition, we also investigated the stability of hydrogen peroxide in solutions. Results indicate that hydrogen peroxide is stable in acidic solutions but unstable in basic solutions. In the alkaline pH range hydrogen peroxide may decompose to give oxygen and water, losing its oxidation ability.

## **II. SOIL CHARACTERIZATION**

The soil samples from three industry sites in two depth ranges (2'~4' feet and 8'~14' feet) were received and pertinent physical-chemical properties, such as pH, specific surface area, moisture content, organic matter content, hydraulic conductivity, cation exchange capacity (CEC), pH at zero point of charge ( $\text{pH}_{\text{zpc}}$ ), particle size distribution and organic contaminants and heavy metals fractionation were analyzed.

### **II.1. Composition Analysis**

Table 2.1 shows the results of composition analysis obtained by using the sedimentation method (Appendix A. 1.) for the soil samples received. Clay and silt are the major components in all soil samples which indicates that the application of electro-osmosis technology will be feasible for these soils.

### **II.2. Soil pH**

The soil pH values were measured by using 0.01 M  $\text{CaCl}_2$  as electrolyte. The results shown in Table 2.1 indicate that most of the soil samples are in the neutral region (pH from 6.1 to 7.6) and the pH variation with depth is insignificant. The method is described in Appendix A.2.

### **II.3. Soil Organic Matter**

Organic matter is an important component of the soil system. It can affect other soil physical properties such as specific surface area, chemical adsorption capacities, and CEC. Table 2.1 shows the results of organic matter content . The analytical method is described in Appendix A.3.

### **II.4. Soil Effective Cation Exchange Capacity**

Table 2.1 shows the results of effective cation exchange capacity (ECEC) of soil samples, the measured ECEC range is from 13.8 to 21.2 meq/100g. The experimental procedures for determination of ECEC are presented in Appendix A.4.

## II.5. Moisture Content

The moisture content results are shown in Table 2.1 . The moisture content range is from 10.2 % to 16.9 %. The analytical method is described in Appendix AS.

## II.6. Specific Surface Area

Figures 2.1 to 2.6 show the results of dye adsorption of all soil samples analyzed. Table 2.1 summarizes the specific surface area of samples tested. The specific surface area data will be useful for future work on organic compounds adsorption and electro-osmosis experiments. The method is described in Appendix A.6.

## II.7. $pH_{ZPC}$

It has been reported in the literature that the electro-osmotic water flow is direct proportional to the zeta potential (Sims and Heckendom , 1991):

$$Q_e = \frac{\epsilon \zeta \phi}{4\pi \eta L}$$

where  $\epsilon$ ,  $\phi$ ,  $\zeta$ ,  $\eta$ , and  $L$  are the dielectric constant, electrical field strength, zeta potential, viscosity of the fluid, and distance between electrodes. This equation shows that the electrical property of the soil will directly affect the electro-osmotic process.

Since the application of electro-osmosis will be investigated in this project, it is crucial to know the microscopic electrical properties of the soil samples. Table 2.1 shows the zeta potential for all soil samples tested. The method is described in Appendix A.7.

## II.8. Hydraulic Conductivity and Hydraulic Permeability

Hydraulic conductivity is an important soil property, because the electro-osmosis technique can be applicable to the contaminated soils with low hydraulic conductivity (lower than  $10^{-5}$  cm/set). Hydraulic permeability can be calculated from the following equation:

$$k = \frac{K\mu}{\rho g}$$

where K= hydraulic conductivity

$\mu$ = dynamic viscosity

$\rho$  = the fluid density

g= acceleration of gravity

The results of hydraulic conductivity and hydraulic permeability are shown in Table 2.1. Experimental procedures are presented in Appendix A.8.

## **II.9. Analysis of Organic Compounds in Soils**

Table 2.2 shows the results of qualitative analysis of several organic compounds in the soil samples. Solvent extraction followed by gas chromatography, analysis with mass spectrometry detector was employed. The detailed procedures are described in Appendix A.9.

## **II.10. Analysis of Heavy metals in Soils**

Table 2.3 and Figures 2.7 to 2.10 show the results of fractionation analysis of lead, cadmium, copper, and zinc in soil samples. The fractions represent the exchangeable, sorbed, organic, carbonate and sulfide forms of metals present in the soils respectively. No significant differences in the heavy metals content were observed among all the soil samples.

Table 2.1 Physical-chemical characteristics of soil samples

Soil Sample <sup>a</sup>	A	B	C	D	E	F
Sand (%)	9	23	22	18	14	22
Silt (%)	46	36	37	36	38	47
Clay (%)	45	41	41	46	48	31
pH	6.10	7.46	7.58	7.60	7.60	7.52
ECEC (meq/100g)	14.7	21.2	21.2	21.2	20.5	13.8
Organic Matter(%)	1.81	0.97	0.82	1.07	0.79	1.17
Moisture (%)	16.9	12.4	11.1	12.7	13.6	10.2
Hydraulic Conductivity (10 <sup>-8</sup> cm/s)	9.52	38.8	1.72	48.4	2.49	11.7
C <sub>2</sub> Cl <sub>4</sub> in Soil (µg/kg) <sup>b</sup>	ND	ND	137,116	172,972	ND	9,877
Zeta potential (mV)	-14.7	-17.6	-26.3	-32.8	-35.1	-22.8
pH <sub>zpc</sub>	2.60	2.46	2.48	2.20	2.34	2.18
Hydraulic Permeability(10 <sup>-7</sup> cm <sup>2</sup> )	9.71	39.6	1.76	49.4	2.54	12.0
Specific Surface Area (m <sup>2</sup> /g)	0.9	0.7	0.4	0.6	0.4	0.5

- a: A ( SB009, depth 2'~4' )  
 B ( SB009, depth 9'~11' )  
 C ( SB010, depth 4'~6' )  
 D ( SB010, depth 8'~10' )  
 E ( SB011, depth 4'~6' )  
 F ( SB011, depth 12'~14' )

b: Extraction Method: 2g soil + 8mL hexane + 2mL H<sub>2</sub>SO<sub>4</sub>(1N)

ND: not detectable

Table 2.2 organic compounds in soil samples.

Soil Sample	A	B	C	D	E	F
Aniline		+				
Hexachloroethane		+++				
Pentachlorobutadiene		+++				
Hexachlorobutadiene		+++				
Tetrachloroethylene			+++	+++		++
Decane					+++	
Tetracosane				++		
Undecane		+			+++	

+++: relatively high concentration

++: intermediate concentration

+: relatively low concentration

Table 2.3 Heavy metal fractionation in the soil samples.

Soil Sample	A	B	C	D	E	F
<b>Lead</b>						
exchangeable	51.8	45.2	45.2	45.2	45.2	45.2
sorbed	43.1	43.1	43.1	43.1	43.1	43.1
organic	75.4	86.2	75.4	86.2	75.4	75.4
carbonate	43.1	32.3	32.3	43.1	43.1	43.1
sulfide	25.9	25.9	25.9	32.3	25.9	32.3
<b>Copper</b>						
exchangeable	13.5	12.4	12.4	12.4	12.4	11.2
sorbed	10.9	10.9	9.0	10.9	10.9	10.9
organic	22.6	24.5	12.9	3.2	ND	ND
carbonate	ND	ND	1.3	1.3	1.3	1.3
sulfide	10.0	11.2	8.9	10.0	11.2	10.0
<b>Cadmium</b>						
exchangeable	5.1	5.4	3.8	3.0	2.7	1.9
sorbed	2.6	1.9	1.9	1.3	2.6	1.3
organic	8.4	7.8	5.8	1.3	ND	ND
carbonate	ND	ND	ND	ND	ND	ND
sulfide	ND	ND	ND	ND	ND	ND
<b>Zinc</b>						
exchangeable	3.3	3.3	3.3	3.0	3.0	2.7
sorbed	2.3	2.3	1.7	1.7	1.7	1.7
organic	5.1	6.2	4.5	4.5	4.5	4.5
carbonate	1.1	2.3	1.1	0.6	1.1	1.7
sulfide	2.0	2.7	1.7	2.0	2.4	2.4

Note: concentrations in mg/Kg  
 ND: not detectable

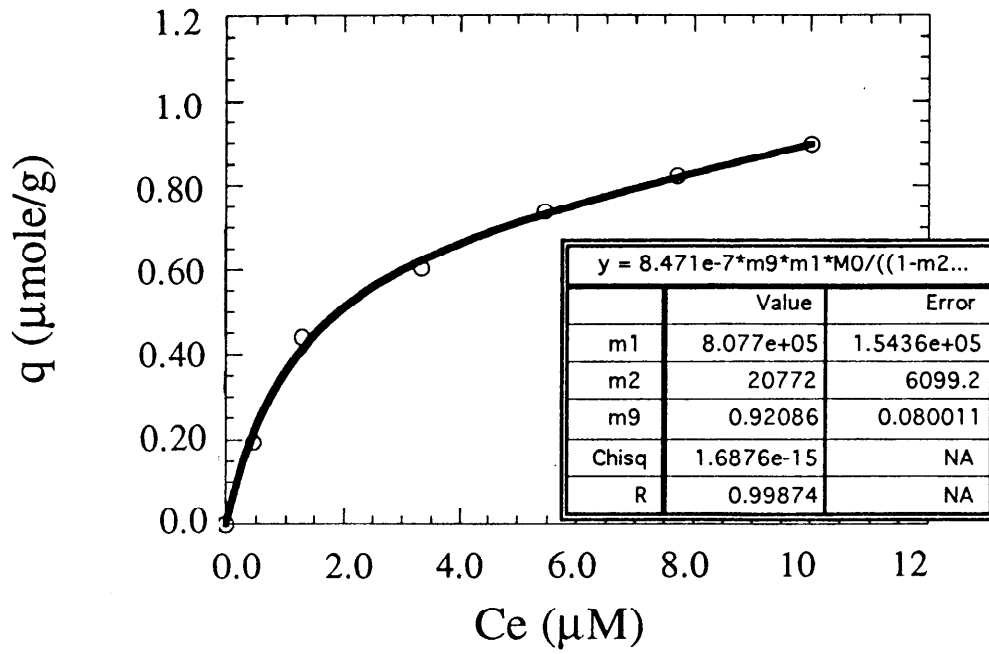


Figure 2.1 Specific Surface Area of Soil-A

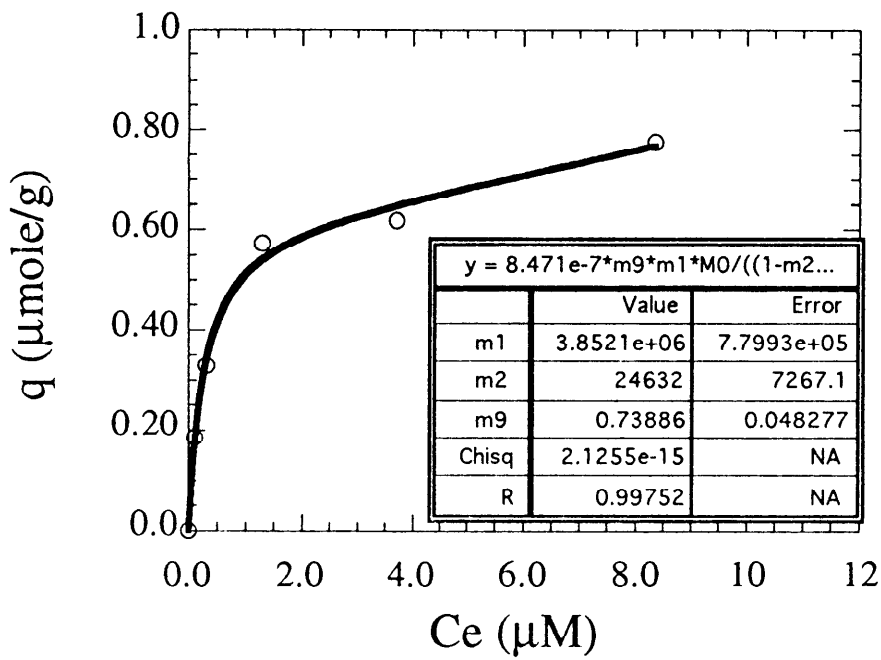


Figure 2.2 Specific Surface Area of Soil-B

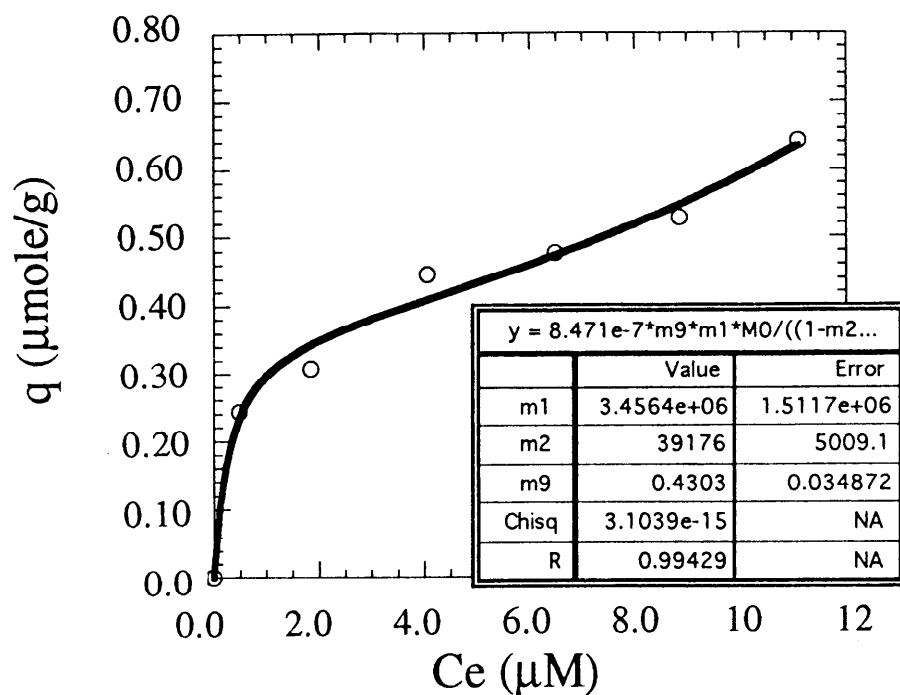


Figure 2.3 Specific Surface Area of Soil-C

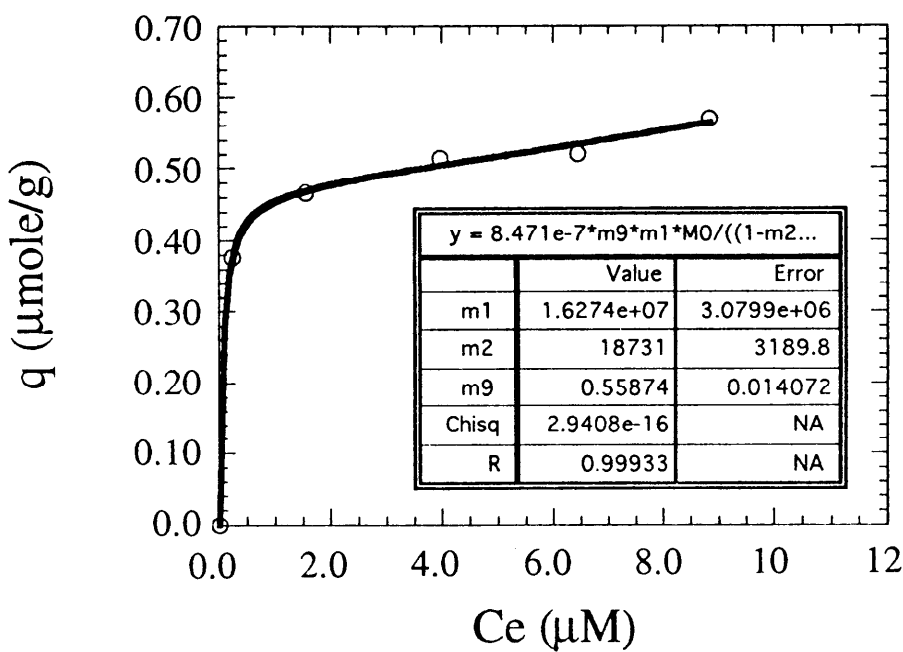


Figure 2.4 Specific Surface Area of Soil-D

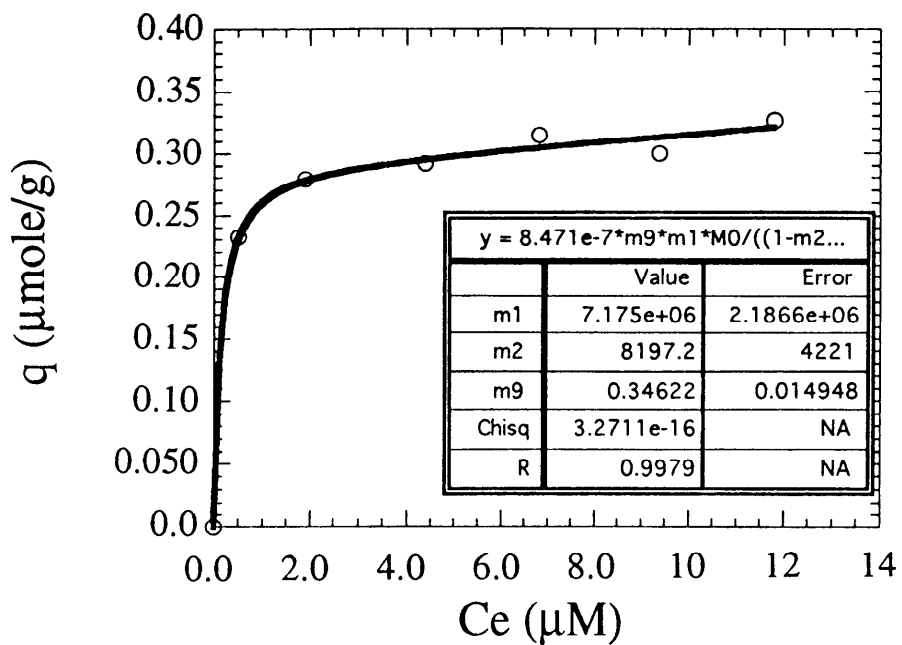


Figure 2.5 Specific Surface Area of Soil-E

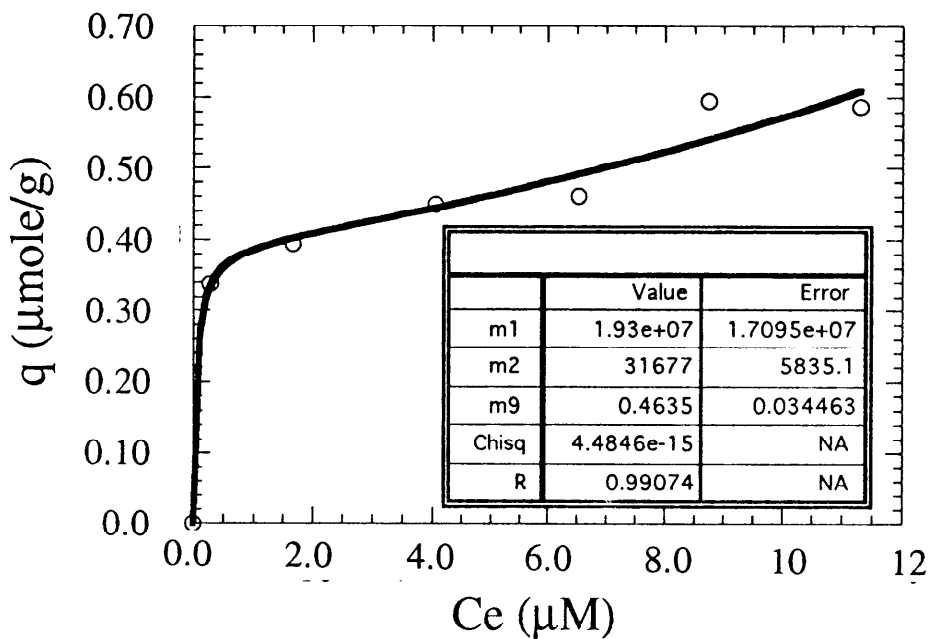
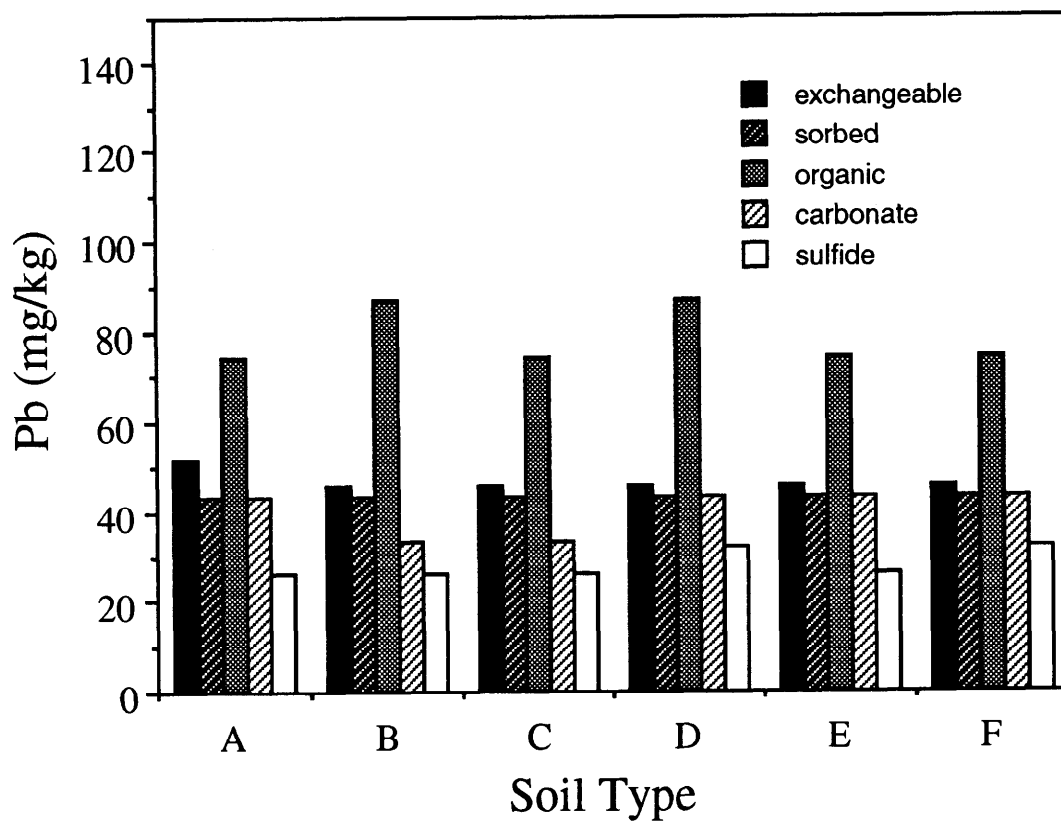
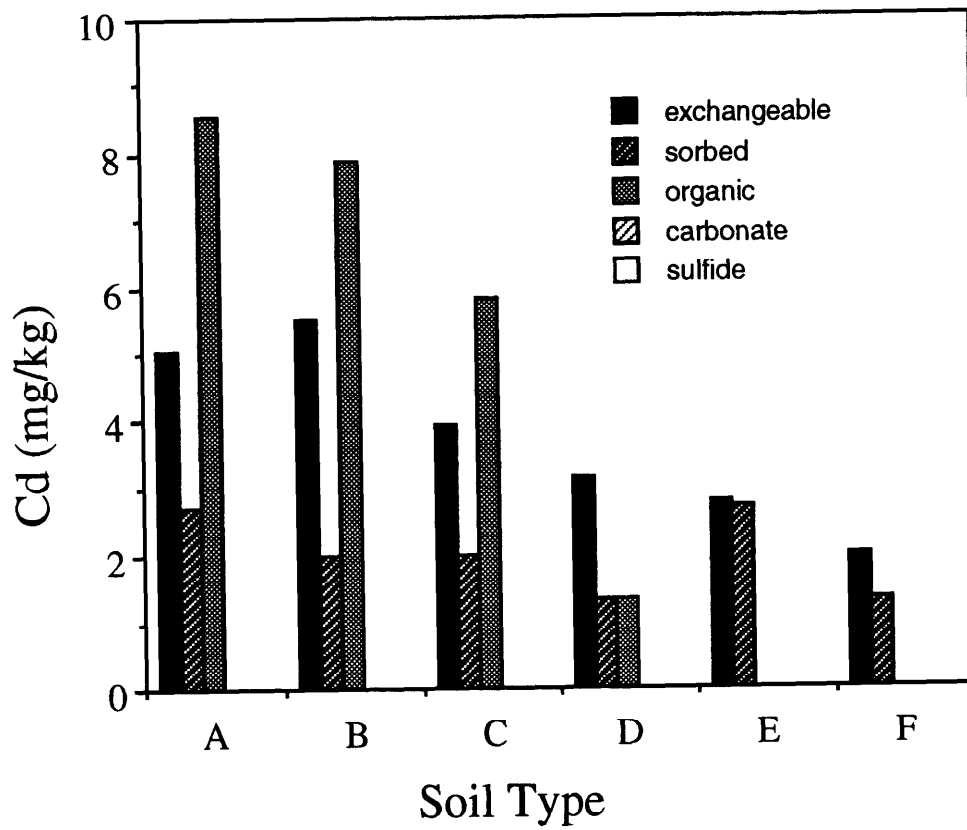


Figure 2.6 Specific Surface Area of Soil-F



**Figure 2.7 The fractionation of Pb in soil samples**



**Figure 2.8 The fractionation of Cd in soil samples**

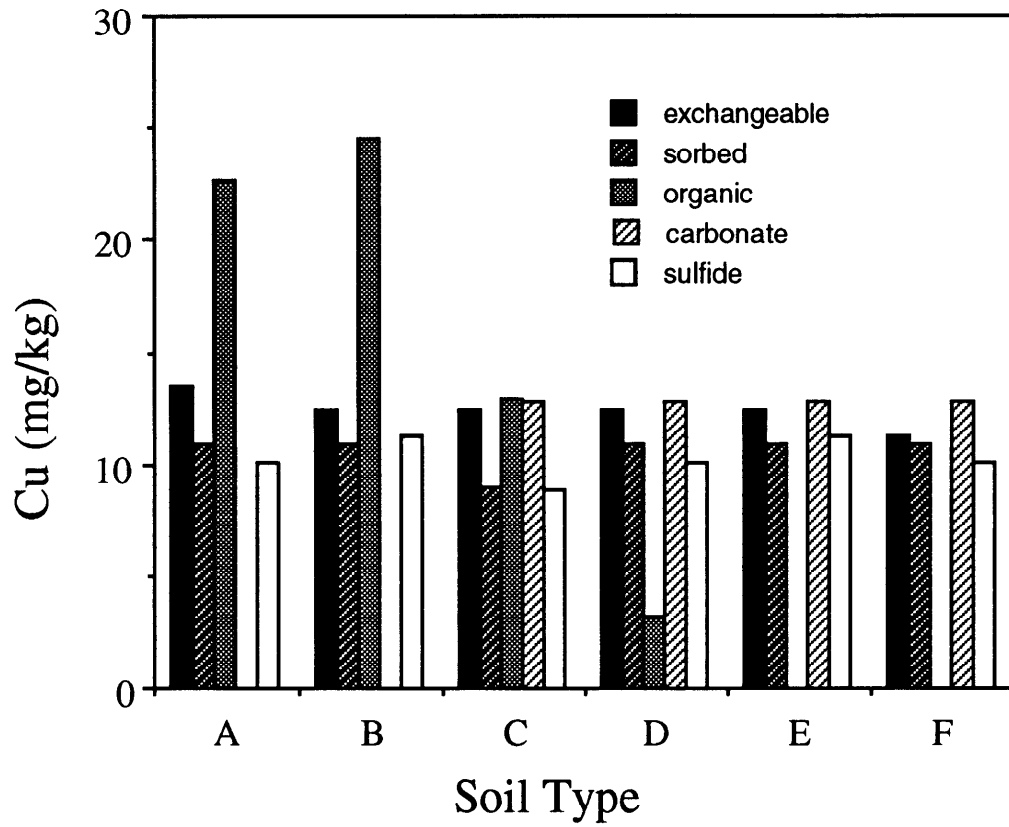


**Figure 2.9 The fractionation of Cu in soil samples**

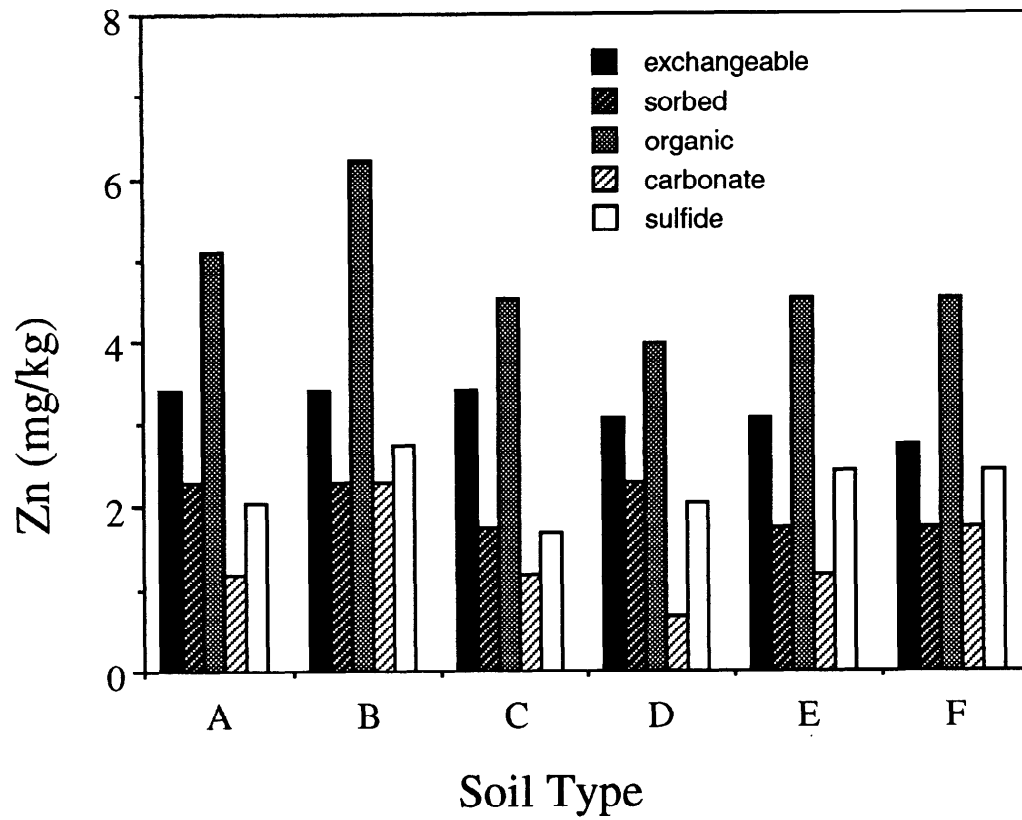


**Figure 2.10** The fractionation of Zn in soil samples

# III. ADSORPTION OF SELECTED ORGANIC COMPOUNDS ON SOILS

## III.1. Experimental Methods

Batch adsorption experiments were conducted at various soil : water ratios (by weight) (1:3 to 1:20) and initial organic compounds concentrations (4-chlorophenol, 2,4-chlorophenol and 2,4,5-chlorophenol ). The procedures were as follows.

To a series of glass bottles, the desired amount of kaolinite and organic compounds solution in 0.05M (NaNO<sub>3</sub>) ionic strength electrolyte were added. The bottles were placed in a shaker. After shaking for 24 hours, the mixtures were centrifuged to removed the solids material and analyzed for the residual organic compounds concentration.

Concentrations of phenols were measured spectrophotometrically on a spectrophotometer at the corresponding optical absorbance. Samples were diluted in acidic ethanol to give absorbances less than 1.2 except for some measurements of 2-chlorophenol which were done in basic methanol.

## III.2. Experimental Results

Adsorption isotherms for phenols with varying chlorine substitution are shown in Figure 3.1. The isotherms show saturating binding as the concentration of phenol is increased and they can be fitted by the Langmuir equation:

$$\Gamma = Q_0 \frac{bC}{(1 + bC)}$$

Constants for the series of phenols obtained from non-linear least square fits of data such as the data shown Figure 3.1 are presented in Table 3.1. For phenol the binding is weak and only 0.6  $\mu\text{mol/g}$  is adsorbed at 8 mM phenol. Thus only the product  $Q_0b$  can be determined. The values of  $Q_0$  are approximately the same for the series of chlorophenols indicating a common mode of binding. If the molecules are assumed to bind in an orientation in which the plane of the phenol ring is parallel to the adsorbing surface the area covered is 1.2- 1.85  $\text{m}^2/\text{g}$  assuming a surface area of 0.532  $\text{nm}^2/\text{molecule}$  (Lu, et al., 1988). Since the surface area of the kaolinite is 6.9  $\text{m}^2/\text{g}$  only a portion of the surface is covered with phenol.

Kaolinite, a two layer clay, has been proposed to have three classes of surfaces (Pefferkom, et al., 1987 ): an aluminum oxide surface like gibbsite, a silica surface and ‘edge’ surface. The silica surfaces are charged at pH above 2 while the alumina surfaces have a  $pK_{ZPC}$  about 9. Binding of monophenols to alumina surfaces is weak (Holmes-Farley, 1988). Binding occurs only upon proton dissociation to form the phenolate. Adsorption is enhanced for catechol and a bidentate complex with the phenolate is suggested (McBride and Wesselink, 1988). The properties of the kaolinite surfaces suggest that binding of phenols is predominantly at the edge surfaces which have been measured to comprise about 15 to 35% of the total surface area (Lee, et al., 1991; Denoyel and Rouquerol, 1991). Our results are consistent with those reported by other researchers. It should be noted that the ‘edge’ surfaces depend upon sample environmental history and may arise from depodition of colloidal silica and alumina on basal faces (Ferris and Jepson, 1975; Diz and Rand, 1989). The edge binding surfaces may be isolated from each other, consistent with the Langmuir nature of the binding which presupposes interaction of bound molecules with the surface alone and not with each other.

In order to test whether the binding of phenols is occurring through equilibration of the surface and the protonated form, the pH dependence of binding was determined for 3 representative chlorophenols with different amounts of chlorine substitution (Figure 3.2). The data are consistent with binding of the protonated species; the experimental values can be fit by assuming that the free concentration of unionized phenol  $[CIPh]_0$  is related to the total phenol concentration,  $[CIPh]_t$ , by the following expression:

$$[CIPh]_0 = \left( \frac{[H^+]}{[H^+] + K_a} \right) [CIPh]_t$$

This value is then inserted in the Langmuir equation using the same constants as in Table 3.1 to generate the curves given in Figure 3.2. The agreement with the experimental binding data demonstrates that binding is predominantly from the protonated species. The data for 2,4-dichlorophenol and 2,4,5trichlorophenol indicate that the binding does not change when the “edge” surface is titrated ( $pK_a=5.9$ ).

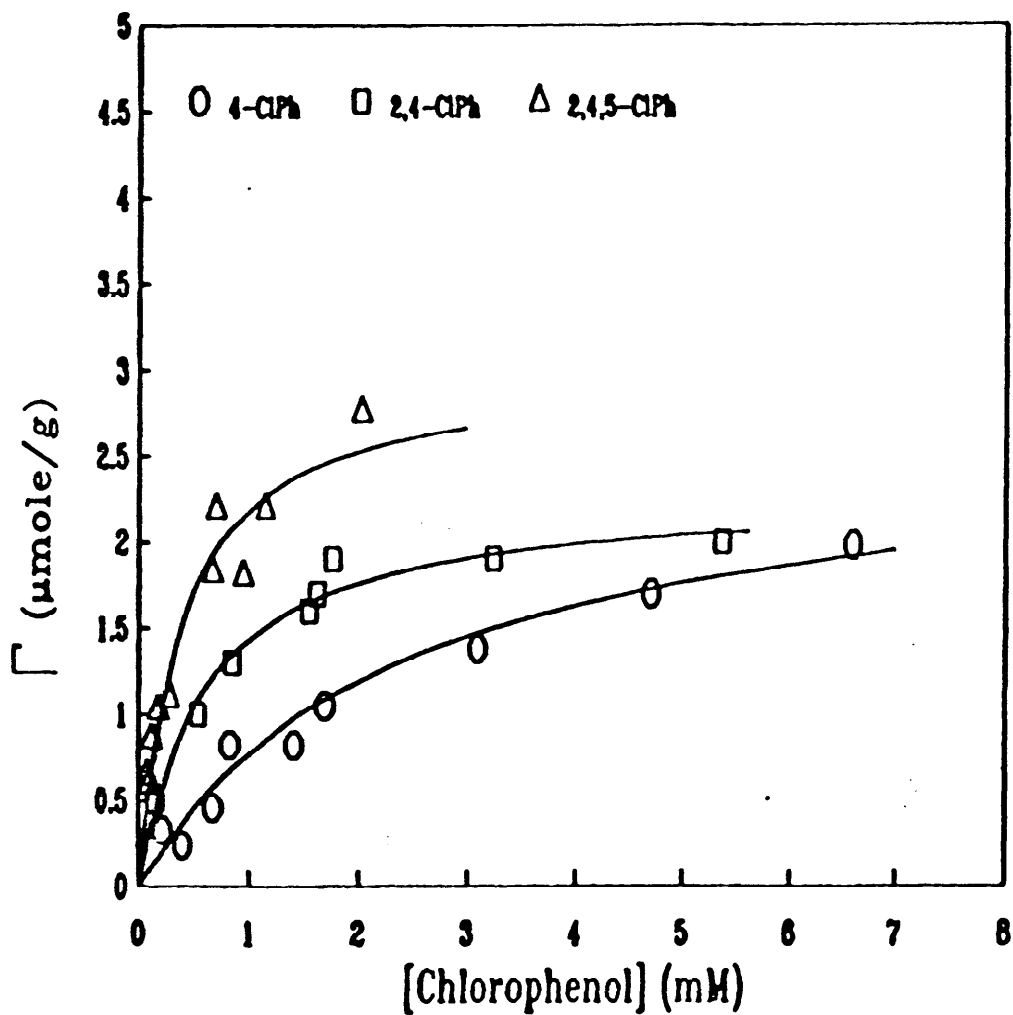


**Figure 3.1** Binding of representative chlorophenols to kaolinite. The amount of chlorophenol bound was obtained from the difference between total chlorophenol added and the free concentration at equilibrium for kaolinite suspended in  $\text{NaNO}_3$  (pH  $\sim$  4). The lines are fits of the data to the Langmuir isotherm (equation 5) with constants given in Table 3.1.

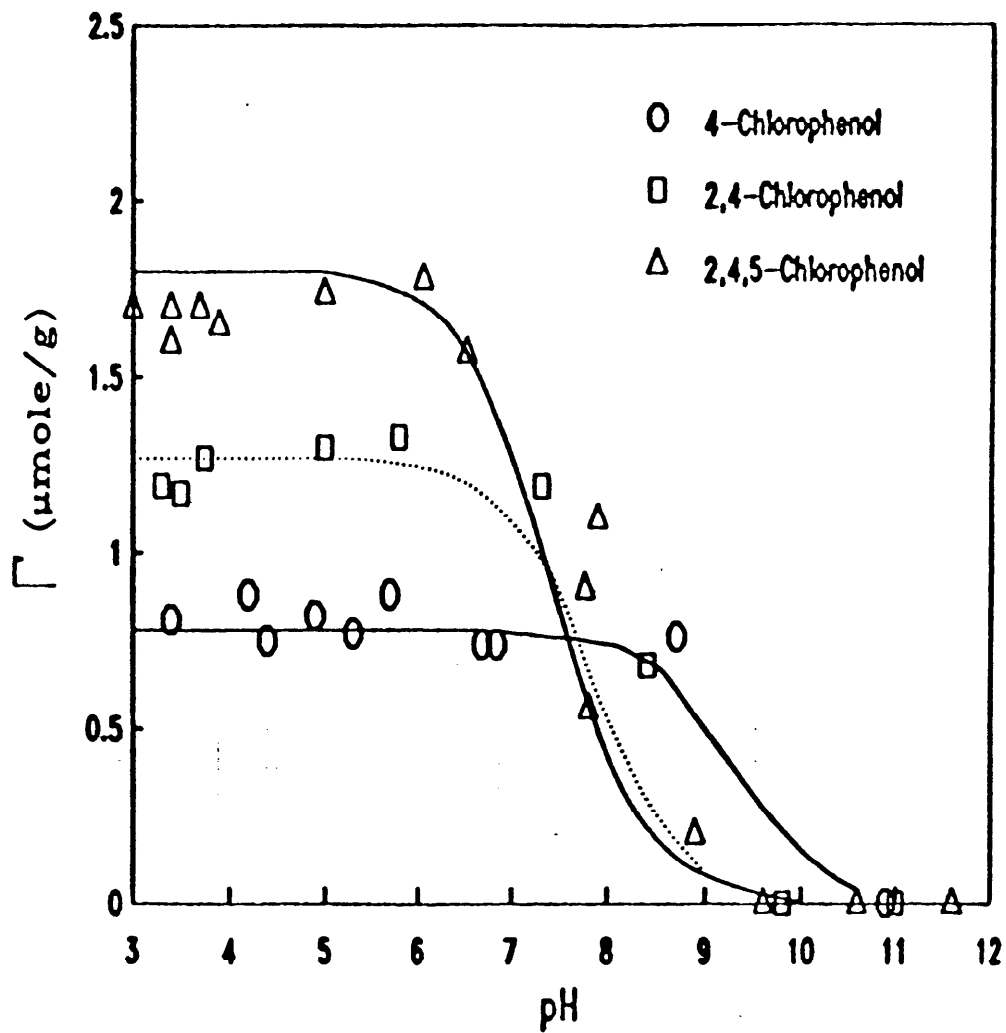


Figure 3.2 The pH dependence of chlorophenol binding to kaolinite, The lines are fits to the data using equation 6 and the  $pK_a$  from Table 3.1.

Table 3.1 Langmuir constants for chlorophenol binding to kaolin ( Constants are calculated by non-linear least squares)

Compound	$Q_0$ ( $\mu\text{mole/g}$ )	$b$ ( $\text{mM}^{-1}$ )
Phenol		0.075 ( $Q_0B$ )
2-chlorophenol	$2.46 \pm 0.12$	$0.42 \pm 0.04$
3-chlorophenol	$2.31 \pm 0.10$	$0.49 \pm 0.06$
4-chlorophenol	$2.61 \pm 0.10$	$0.42 \pm 0.10$
2,3-dichlorophenol	$3.42 \pm 0.25$	$0.72 \pm 0.14$
2,4-dichlorophenol	$2.28 \pm 0.05$	$1.69 \pm 0.14$
2,5-dichlorophenol	$3.49 \pm 0.05$	$0.60 \pm 0.02$
2,6-dichlorophenol	$2.8 \pm 0.3$	$0.85 \pm 0.24$
3,4-dichlorophenol	$2.75 \pm 0.13$	$1.82 \pm 0.32$
3,5-dichlorophenol	$2.25 \pm 0.10$	$1.49 \pm 0.19$
2,4,5-trichlorophenol	$3.0 \pm 0.2$	$2.3 \pm 0.3$
2,4,6-trichlorophenol	$2.76 \pm 0.13$	$2.07 \pm 0.26$

## IV. ELECTRO-OSMOSIS EXPERIMENTS

### IV.1. Experimental Methods

Four electro-osmosis experiments were conducted using various phenolic compounds. Soils contaminated with phenol, 2-chlorophenol, 3-chlorophenol and 4-chlorophenol were utilized and the same experimental procedures were applied to all of the tests. Table 4.1 below shows some of the experimental conditions of the electro-osmosis tests performed with phenolic compounds.

Table 4.1. Some experimental conditions of the electro-osmosis tests with phenolic compounds.

Test #	Contaminant	Concentration (ppm)	Potential Gradient Applied (V/cm)
Blank	none	0	1.2
ph	phenol	166	1.2
2Clph	2-chlorophenol	143	1.2
3Clph	3-chlorophenol	143	1.2
4Clph	4-chlorophenol	143	1.2

Figure 4.1 shows the electro-osmosis apparatus employed to perform the experiments. The electro-osmosis cell consisted of an acrylic unit with a central cylinder of 11.5 cm in length and 8.9 cm in internal diameter where the soil samples were placed. The volume of both cathode and anode compartments were 700 mL. To separate the soil from the water solution, a set of two nylon meshes (Spectrum; model PP, mesh opening 149  $\mu\text{m}$ ) with a filter paper (Whatman; qualitative) in between were used as a membrane in each of the electrode reservoirs. Graphite rods (Ultra Carbon Co.; type ultra "F" grade 014144-08 U7/SPK; 0.615 cm in diameter) were utilized as electrodes and a series of 8 rods were held at each compartment near the central cylinder, right behind the membranes.

The soil was a combination of Ottawa sand (U.S. Silica Company) and Georgia kaolinite (Georgia Kaolin Company) at ratio 1: 1 (w:w). A solution of the phenolic compound (in NaCl  $10^{-3}$  M) was mixed well with the dry soil and let stand for about 24 hours to reach an equilibrium and consequently provide an uniform distribution of the contaminant in the soil

system. The mixture was then carefully packed in the acrylic cylinder to avoid formation of large air spaces.

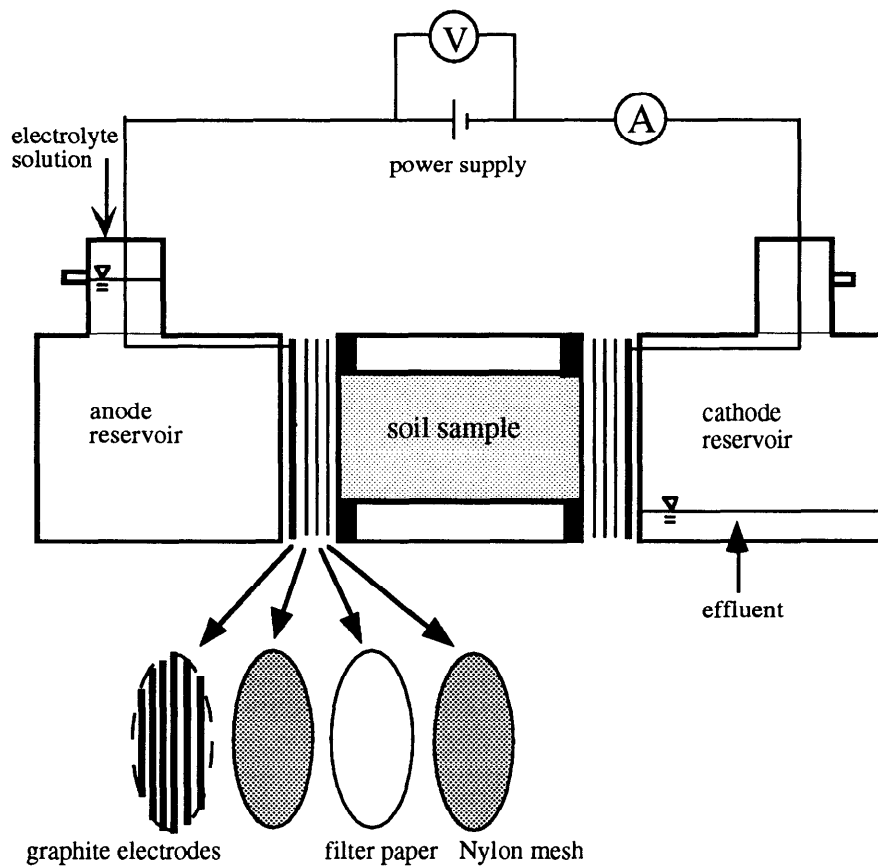


Figure 4.1. Schematic diagram of the electro-osmosis laboratory apparatus.

To begin the tests, the electrodes were connected to a 12 volts DC power supply (Power/Mate Corporation; model E- 12/158). The anode container was kept filled with NaCl  $10^{-3}$  M electrolyte solution and the cathode compartment was initially empty. Daily water samples were taken at the cathode side and during the experiments parameters such as amount of water flow, current, effluent contaminant concentration, pH of catholyte and anolyte were monitored as a function of time.

At the conclusion of test, the soil samples were removed from the cell and sliced into 10 sections. Each one was then analyzed for water content, pH and contaminant concentration.

## **IV.2. Experimental Results**

### **IV.2.1 Electra-Osmosis Water Flow**

Figure 4.2 shows the amount of electro-osmotic flow produced as a function of time. In general, the flow reached a maximum value and then decreased gradually possibly due to changes in the electrical properties of the packed soil cores originated from the electrochemistry associated with the electro-osmosis process. By applying a potential to the system, water decomposed to  $H^+$  and  $O_2$  at the anode and these hydrogen ions flushed across the cell modifying the original conditions of the pore fluid. Simultaneously, vigorous production of  $OH^-$  took place at the cathode because of the electrochemical reduction of water. Accounting for these occurrences, the hydraulic properties of the soil could be altered by dissolution of salts and clay minerals, adsorption/desorption interactions, precipitation of metal hydroxides and cation exchange (Hamed et al., 1991). The complexity of the soil system turned very difficult to interpret the specific causes of the changes of the electrical properties soil core. Pamukcu and Khan (1989) suggested that reversing the current of the electrical system and replacing the electrolyte solutions by fresh solutions would indicate any structural changes in the packed soil. If there are any variations in water flow after these changes, the hydraulic properties of the soil system is believed to be altered with respect of the initial condition. Based on this, the authors demonstrated that no changes in the soil structure was observed during the electro-osmosis process at least for kaolinite and the electrical properties of the pore fluid significantly affected the electro-osmotic water flow. To better illustrate these changes, a plot of current density (current per cross sectional area of flow) versus time is presented in Figure 4.3. It was observed that the current also reached a maximum value at the first days of experiments and then decreased gradually.

A linear correlation was found between the average water flow and the average current density (Figure 4.4). The higher the current density, the greater was the water flow. The current passing through the soil core was mainly credited to the ions in the liquid phase. Some of these ions (cations) were responsible for the water flow and a high current should evidently yield high electro-osmotic water flow. Therefore, current density could be used as a measurement of the efficiency of electro-osmotic process.

Noticeable differences among the experiments were related to the water flow. Figure 4.5 presents the diagram of accumulative flow versus time. The test with 2-chlorophenol produced the highest flow while the blank test showed the lowest water flow. It was noticed that the water flow was also related to the pore volume of the soil core. The larger the pore volume, the larger was the electro-osmotic water flow since more water was available to be transported. Obviously there is a limitation in this occurrence; if the pore volume is too large (see blank test), the system behaves as a free electrolyte solution and less electro-osmotic flow is recorded (Kezdi, 1980). Figure 4.6 exhibits the average flow in total of each experiment versus pore volume. The average flow increases with increasing pore volume until a point then decreases abruptly.

#### **IV.2.2 Coefficient of Electra-Osmotic Permeability ( $k_e$ )**

Figure 4.7 shows the changes of the coefficient of electro-osmotic permeability ( $k_e$ ) as a function of time. As expected, the pattern is similar as for the electro-osmotic water flow since the latter and electro-osmosis permeability are closely related as demonstrated in equation (4.1):

$$Q_e = k_e i_e A \quad (4.1)$$

This equation can be used to estimate the  $k_e$  values of a soil system (Casagrande, 1949). In the present case the potential gradient  $i_e$  and the cross section area  $A$  were constant. The  $k_e$  values were found to be consistent with those reported in the literature (Casagrande, 1949) of about  $10^{-5} \text{ cm}^2/\text{V.s}$ .

#### **IV.2.3. Influent-Effluent pH Changes**

The influent and effluent pH variation during the electro-osmosis experiments are presented in Figures 4.8 and 4.9, respectively. As mentioned previously, hydrogen ions ( $\text{H}^+$ ) were produced from the oxidation of water causing the drop in pH at the anode and hydroxyl ions

(OH) from the reduction of H<sub>2</sub>O were responsible for the pH increase at the effluent. For all experiments the pH at the anode (influent) decreased from values around 5 to approximately 2.5 to 3.0 while the effluent pH (cathode) rose to values between 12 to 13 and then decreased gradually due to the acid front generated at the anode. It is well known that hydrogen ions have higher mobility than hydroxyl ions (Acar and Alsahwabkeh, 1993). Thus, hydrogen ions move towards the cathode faster (due to its higher electrochemical mobility and convection) than the hydroxyl ions to the anode and a decrease in pH would be expected at the cathode solution.

#### **IV.2.4. Contaminant Removal**

Figures 4.10 and 4.11 present the percent contaminant removal as a function of time and the percent removal related to the total water volume flushed through the soil cores (in units of pore volumes of flow), respectively. The results demonstrated that good contaminant removal was achieved from the cathode side. For these experiments, no samples of the anode were analyzed for contaminant concentration. The 2-chlorophenol was almost completely removed from the soil (94 %) while only 58 % of the phenol was carried out by the electro-osmosis process. The removal of 3-chlorophenol and 4-chlorophenol were 85 % and 79 %, respectively. In Figure 4.11, one can observe that the removal efficiency was proportional to the amount of water passed through the soil samples. The greater the amount of liquid flushed through the soil, the greater was the contaminant removal. Acar and Alsahwabkeh (1993) demonstrated that high removal of phenols from kaolinite were achieved by passing at least 2 pore water volumes through the soil. High removal were observed in the tests with 3-chlorophenol and 2 chlorophenol and Figure 4.11 shows that more than 2 pore water volumes were flushed through the simulated contaminated soil. All the tests were run for 13 to 17 days and the differences in contaminant removal were greatly affected by the fluid velocity through the soil. The test with 2-chlorophenol presented the highest removal and average fluid velocity. It is crucial to understand factors influencing the fluid velocity (or water flow rate) of the electro-osmotic process. Results from this study indicate that physical properties of the soil core are very important.

#### **IV.25 The pH Profile, Water Content and Contaminant Distribution**

After the completion of the tests, the samples were sliced into 10 sections and analyzed for pH, water content and contaminant concentration. The resulted pH profiles for the 5 tests performed shown in the Figure 4.12 were originated exclusively from the redox reactions of water at the electrodes and demonstrated to have the same pattern as the profiles determined by Hamed et al. (1991). The acidic electrolyte solution generated at the anode reservoir flowed across the soil

sample lowering the pH to values around 3 to 4 until near to the cathode the pH rose to values about 8 to 9 because of the basic conditions produced by the reduction of water.

Water content was measured in order to determine the concentrations of the phenolic contaminants per gram of dry soil and it was found to have almost an uniform distribution across the cell with an average value of 14 to 15 % as presented in the Figure 4.13. The section closest to the anode presented higher water content than the other sections. This result was expected since the liquid flow was directed towards the cathode and water was supplied continually at the anode side.

Figure 4.14 shows the distribution in relative concentration of the phenolic compounds remained in the soil. Small amounts of 4-chlorophenol and high concentration of phenol were retained while no 2-chlorophenol and 3 chlorophenol were found in the soil. An accumulation of phenol above the initial concentration (represented by the solid straight line at  $C/C_0$  value of 1) was detected near the cathode, indicating that the contaminant does not move uniformly across the soil core. At high pH conditions (such as in the vicinity of the cathode), the phenol molecules ( $pK_a = 9.9$ ) were in the unprotonated form, or as anions, and therefore suitable to electromigration towards the anode. Because the water flow rate of the experiment with phenol was low, the electromigration overcame the convective velocity in the region close to the cathode. As a result, high concentration of phenol was detected at that zone. For the other tests, similar accumulation was not observed because the convective velocity was large enough to “push” the contaminants out of the soil. The remaining contaminant concentration of the phenolic compounds tested do not appear to be affected by the compound type since all the mono-chlorophenols possess similar physical properties. As discussed above, the fluid velocity plays an important role on the removal of pollutants from soil by electro-osmosis and the test for phenol presented the lowest average water velocity through the soil.

#### **IV.2.6. Mass Balance**

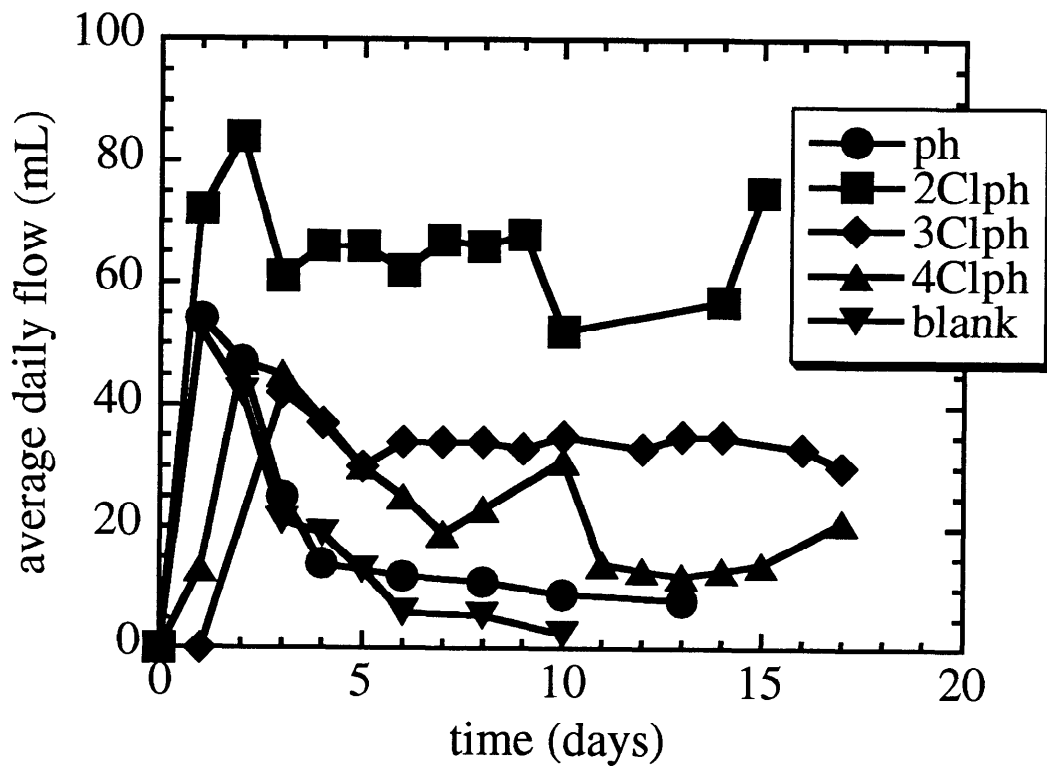
The mass balance for the phenol and mono-chlorophenols are summarized in the Table 4.2. The differences can be attributed to the transport (diffusion and/or migration) of the compounds to the anode reservoir and to the efficiency of the extraction method used to determine the contaminant concentrations in the soil.

Table 4.2. Mass balance for phenol and chlorophenol experiments

Tcst	ph	2Clph	3Clph	4Clph
Mass				
removed from the soil (mg)	120.6	165.5	157.1	144.2
remained in the soil (mg)	81.3	N.D. <sup>a</sup>	N.D. <sup>a</sup>	10.4
total (mg)	201.9	165.5	157.1	154.6
initial mass (mg)	207.0	179.2	183.9	185.0
difference (mg)	5.1	13.7	26.8	30.4

<sup>a</sup> : Not detectable

Analysis of the contaminants at the anode reservoir were not performed in these experiments. Moreover, loss of chlorophenols by volatilization was not monitored. Nevertheless, the results of mass balance were satisfactory.



**Figure 4.2** Electro-osmotic water daily flow for phenol and chlorophenol experiments.

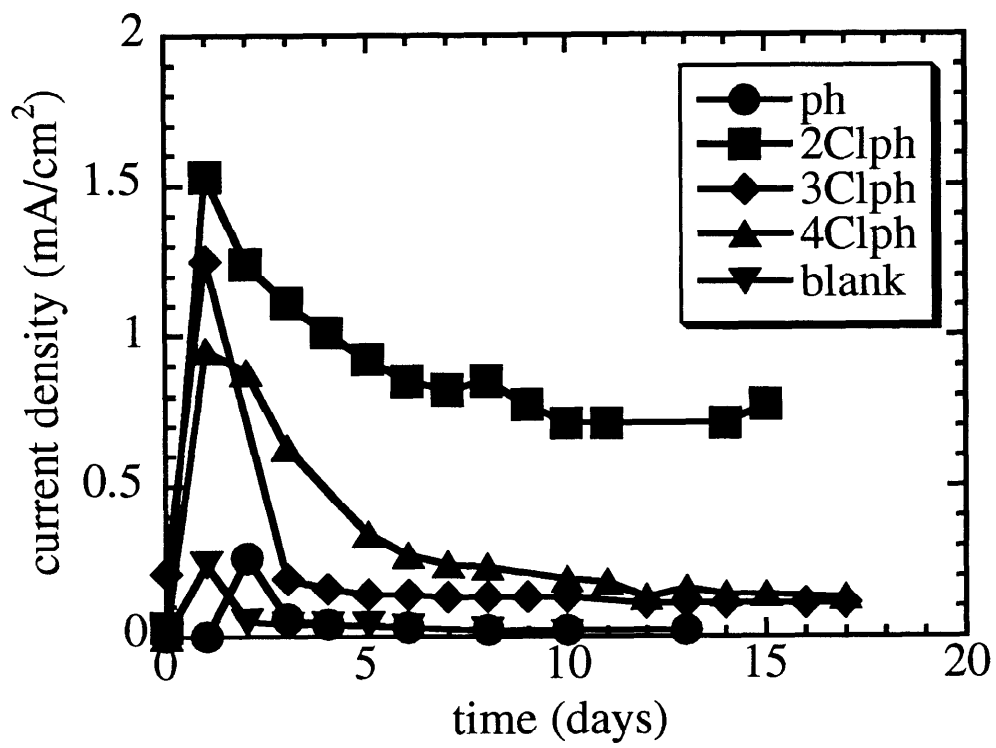


**Figure 4.3** Current density as a function of time for phenol and chlorophenols experiments.

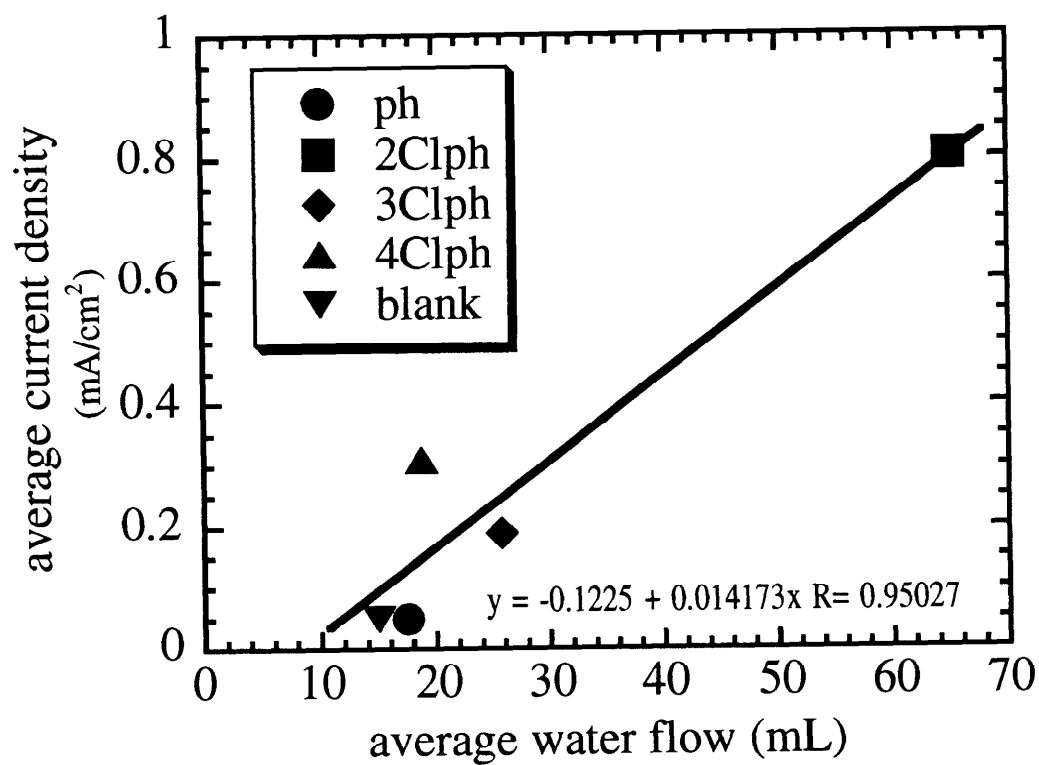


**Figure 4.4 Correlation between electro-osmotic water flow and current density for phenol and chlorophenol experiments.**

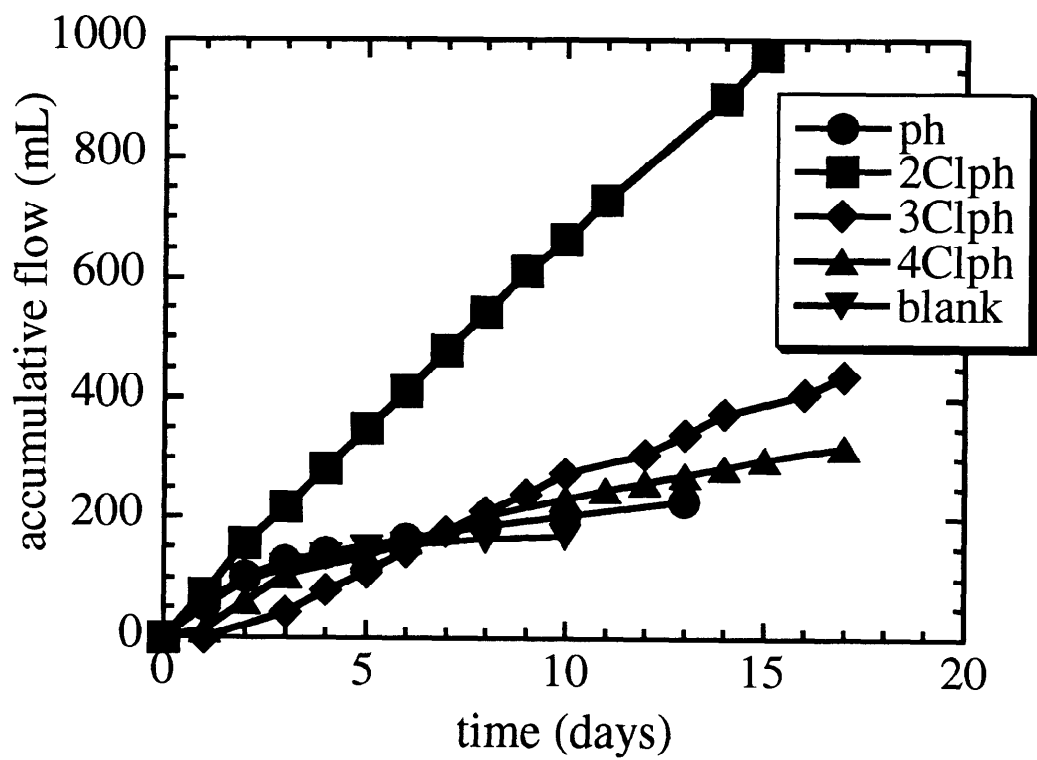


**Figure 4.5 Accumulative electro-osmotic water flow as a function of time for phenol and chlorophenol experiments.**

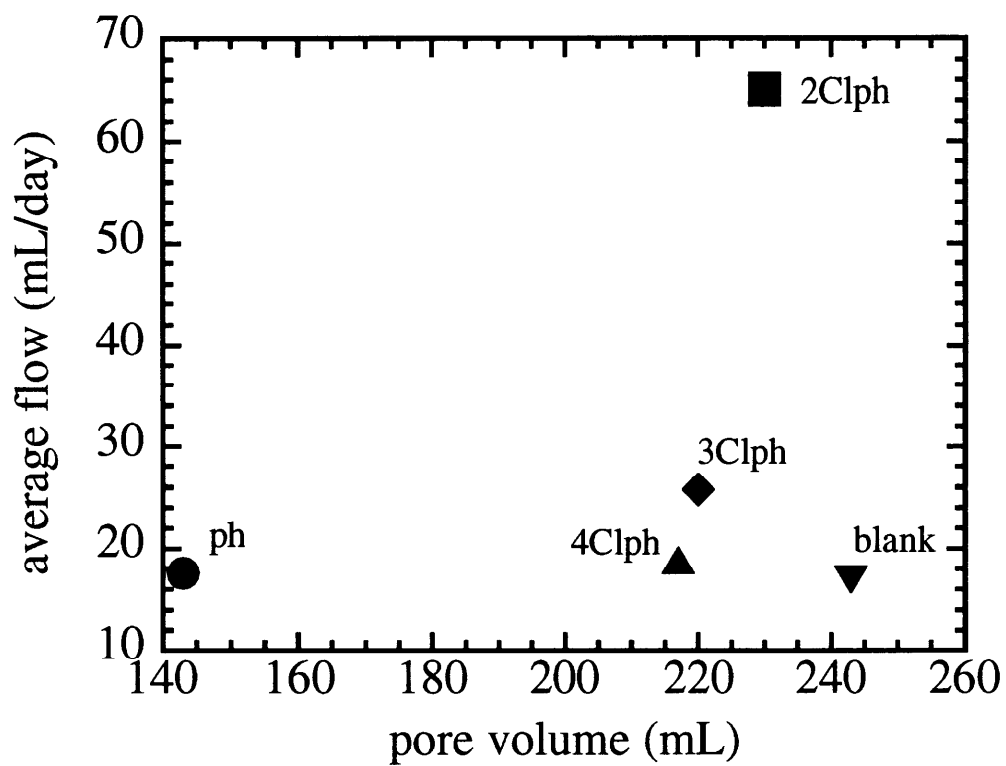


**Figure 4.6 Average electro-osmotic water flow as a function of pore volume for phenol and chlorophenols experiments.**

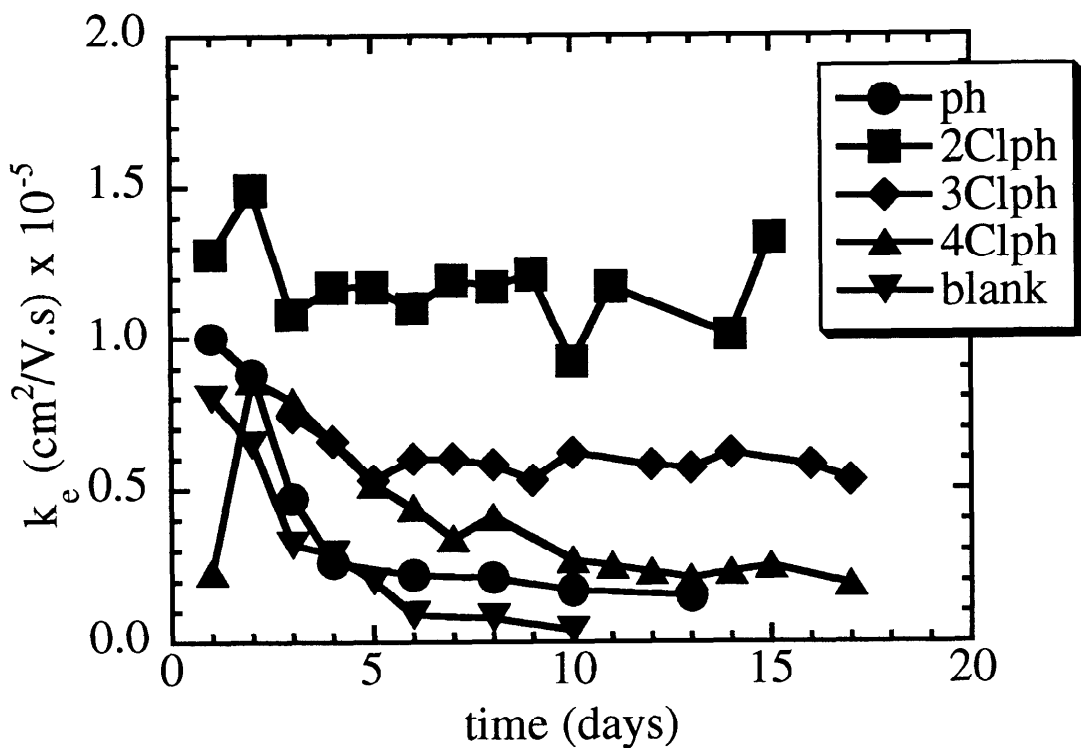


**Figure 4.7 Coefficient of electro-osmotic permeability as a function of time for phenol and chlorophenols experiments.**

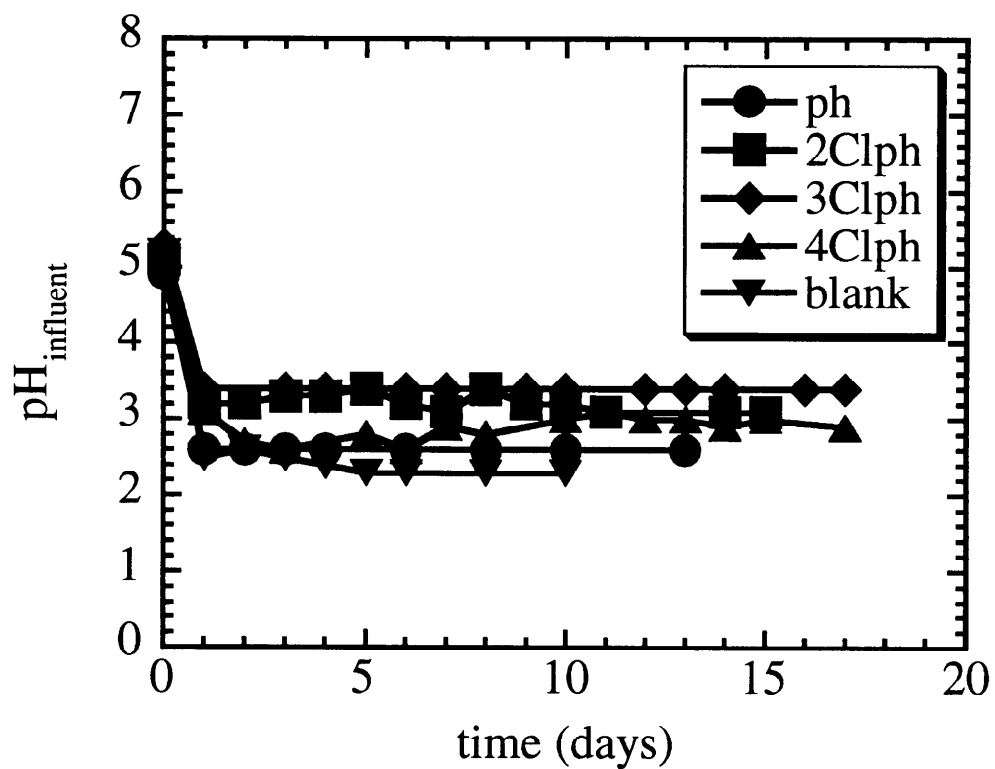


**Figure 4.8** Influent pH as a function of time for phenol and chlorophenols experiments.

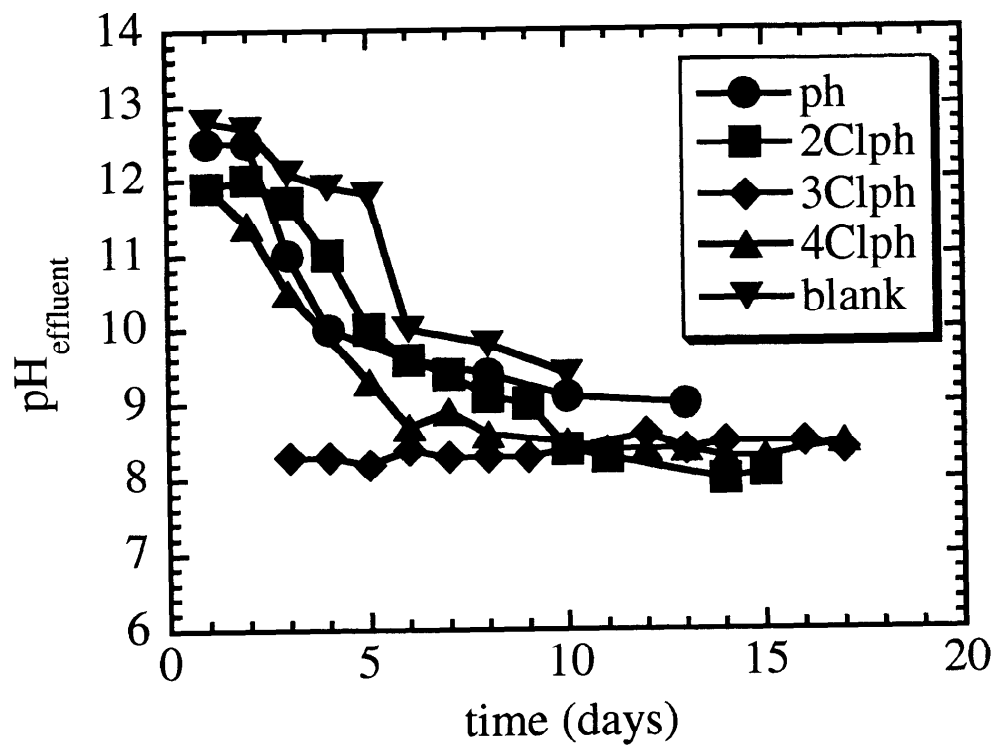


**Figure 4.9 Effluent pH as a function of time for phenol and chlorophenols experiments.**

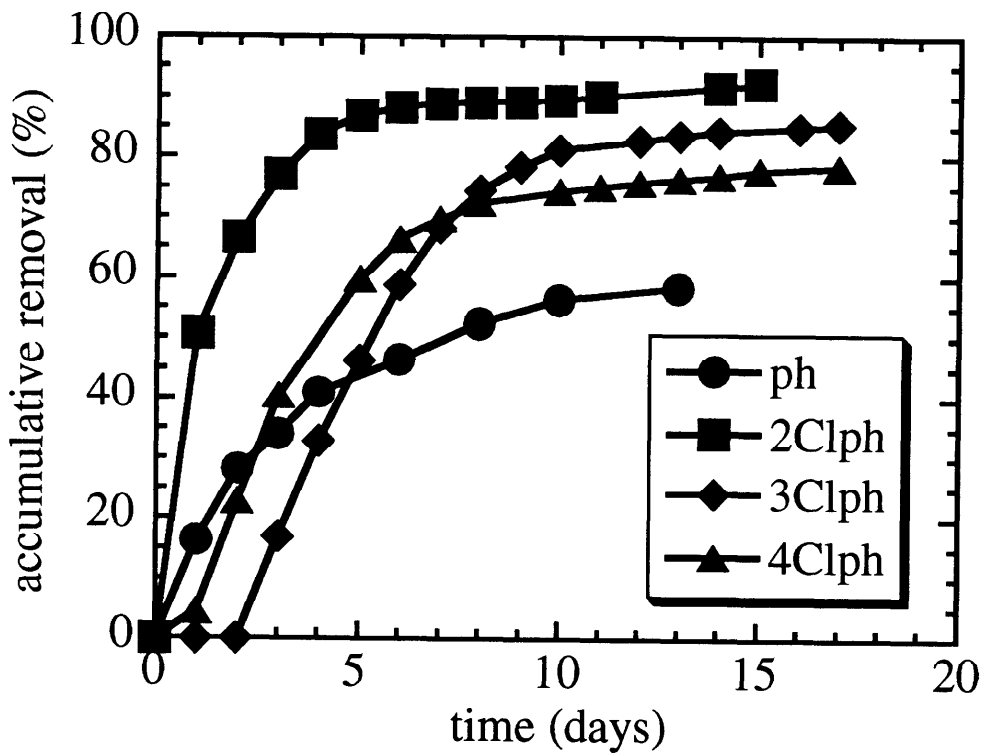


**Figure 4.10** Accumulative removal (%) of phenol and chlorophenols as a function of time.

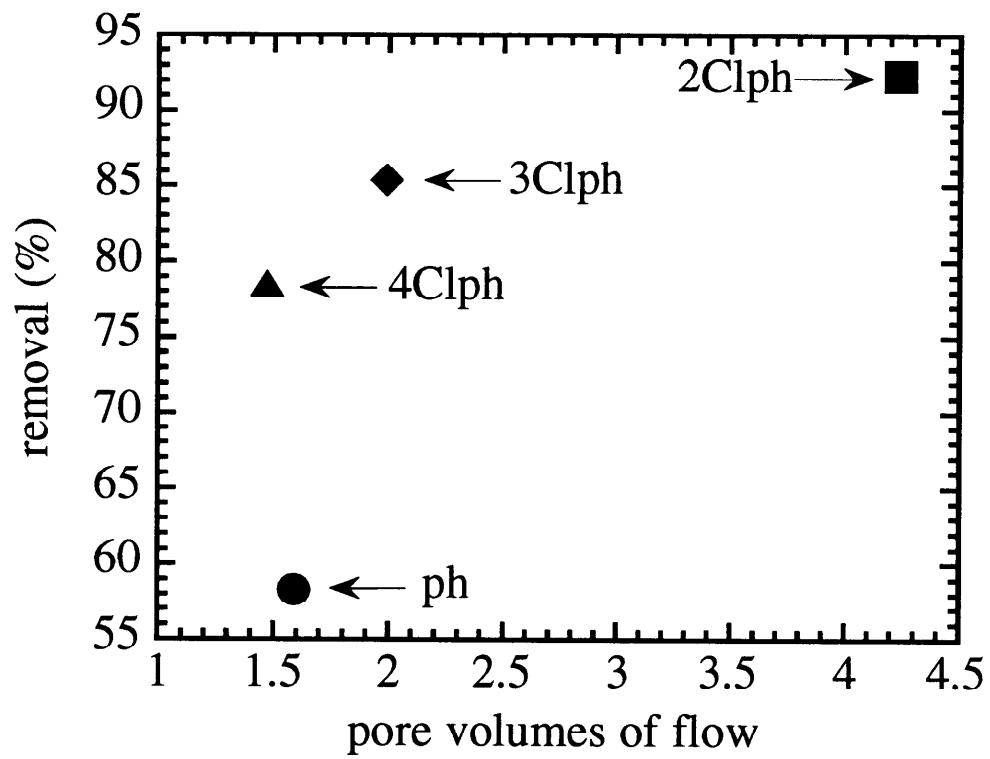


**Figure 4.11** Percentage contaminant removal as a function of pore volumes of flow.

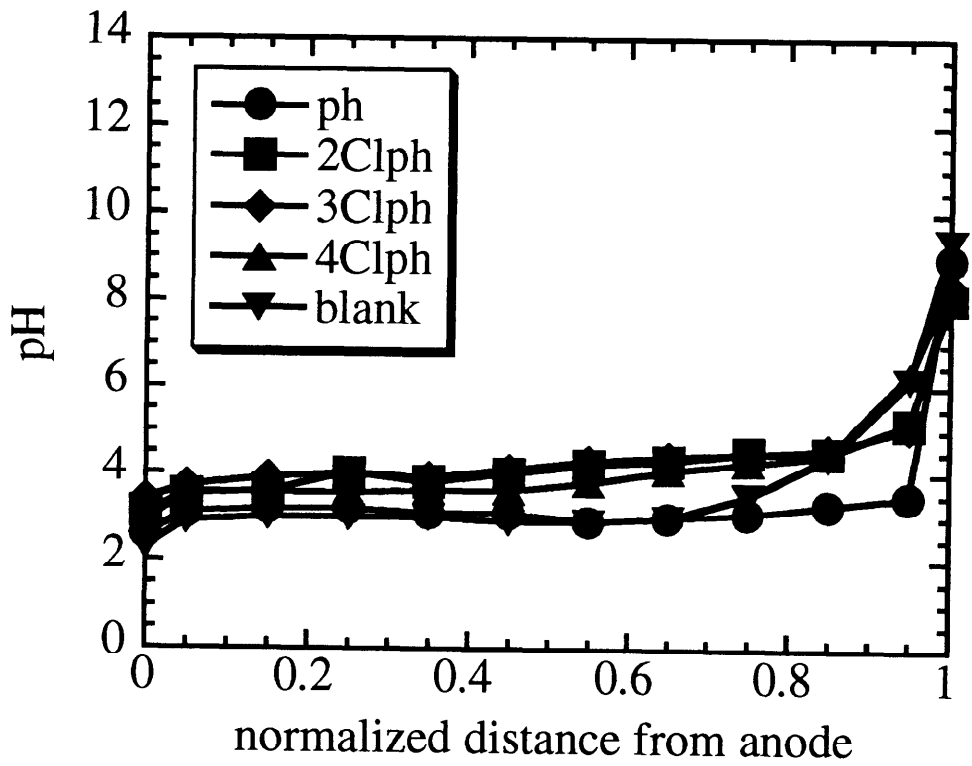


**Figure 4.12** The pH profile as a function of normalized distance from anode for phenol and chlorophenol experiments.

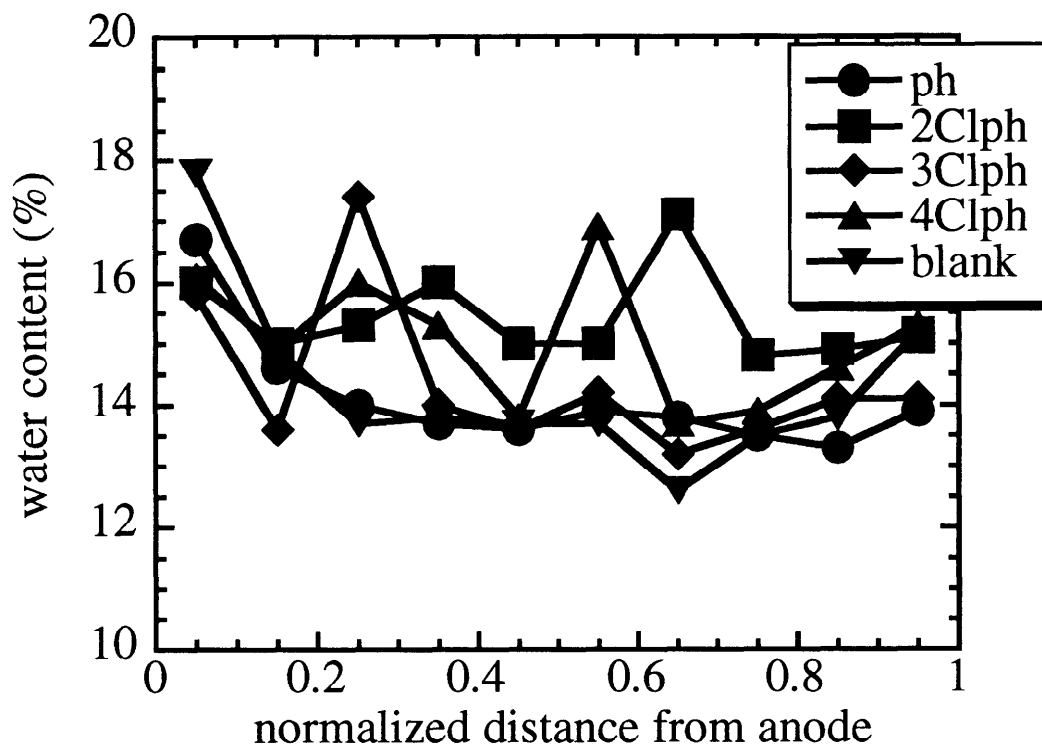


**Figure 4.13** Water content distribution as a function of normalized distance from anode for phenol and chlorophenols experiments.

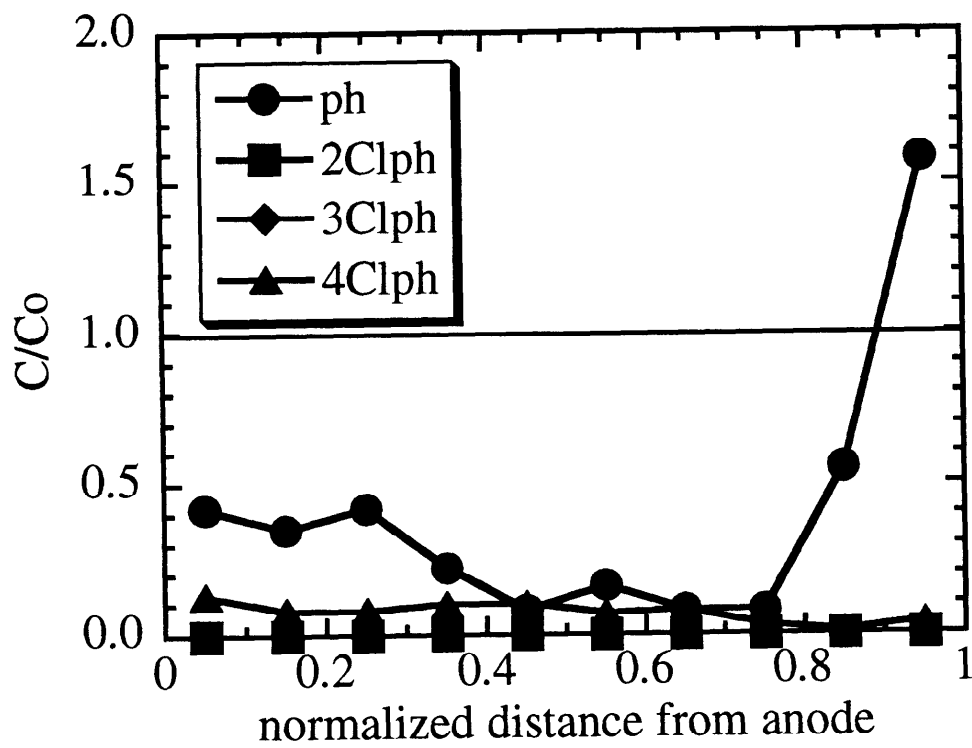


**Figure 4.14** Contaminant distribution through the soil as a function of normalized distance from anode for phenol and chlorophenol experiments.

## V. ELECTRO-FENTON EXPERIMENTS

### V.1. Experimental Methods

#### V.1.1. Reactor Configuration

Table 5.1 shows the dimensions of the reactor utilized for the present research. The anodic chamber is approximately 40% of the total reactor volume, while the cathodic chamber is 60% of the total volume. This means that more than 4.5 liters of waste water or any contaminated water can be treated.

Table 5.1. Reactor dimensions.

Cathodic Chamber	10 x 5 x 5.5 in <sup>3</sup> (254 x 127 x 139.7 mm <sup>3</sup> ) $V_c = 4.51$ L
Anodic Chamber	10 x 3.5 x 5.5 in <sup>3</sup> (254 x 88.9 x 139.7 mm <sup>3</sup> ) $V_a = 3.15$ L
Total Reactor Volume	$V_t = 7.66$ L

#### V. 1.1.1. Electrolysis Cell

Figure 5.1 shows a schematic diagram of the reactor used in this research. The reactor is made of acrylic and it is mainly formed by two chambers: the anodic and the cathodic, in which the anode and the cathode are respectively placed. These two chambers are separated by a cation exchange membrane (Model CMX Neosepta Cation Selective Membrane, Electrosynthesis, E. Amherst, NY). The cation exchange membrane avoids the decomposition of hydrogen peroxide once it is formed in the cathode surface.

In the anodic chamber the oxidation of the water takes place, discharging electrons, oxygen gas, and hydrogen ions into the solution. In the cathodic chamber, oxygen is bubbled into the electrolyte solution and it is electrochemically reduced to hydrogen peroxide. These two reactions are schematically represented in Figure 5.2.

### V. 1.1.2. Electrodes

Two working electrodes, the anode and the cathode, are made of graphite (grade 2020, Carbone of America, Ultra Carbon Division, Bay City, MI).

The anode has a rectangular geometry of 4.0" x 6.0" x 0.1" dimensions with a total available surface area of 48.0 square inches.

Three different cathode geometries as shown in Figure 5.3 are tested to determine the influence of the cathode surface area:

- a) The first cathode geometry is called "plate". It has the following dimensions : 8.0" x 6.0" x 0.1", which means a total surface area of 96.0 square inches for the hydrogen peroxide generation.
- b) The second cathode geometry is called "short finger". Its structure is made of a base plate (with the same dimensions as the plate); four rectangular plates called "fingers" are connected on the base plate. The fingers have a length of 0.4 ".
- c) The last cathode geometry is called "long finger". It has the same structure as the short finger but the finger length is longer: 0.6". The difference in length between these two fingers can contribute to a large difference in the hydrogen peroxide generation.

### V.1.1.3. Oxygen Bubbling System

Oxygen is bubbled directly on to the cathode surface. Two different mechanisms are utilized: a six stone diffusers system and a pipe in which several holes were made. The diffuser system is able to produce smaller bubble sizes while the bubbles generated in the pipe are larger.

The oxygen source is obtained by a compressed oxygen bottle. Air (23% oxygen content) and a 50% oxygen-nitrogen mixture are also tested in order to determine the quantitative amount of oxygen needed for the hydrogen peroxide production.

### **V.1.2. Power Supply and Equipment Configuration**

Figure 5.4 shows a schematic diagram of the laboratory setup for this experiment. The following apparatus are utilized:

- a) A DC power supply to generate the current intensity that flows through the

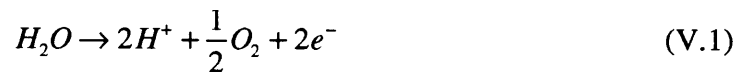
electrodes.

- b) A pH meter and a pH controller to control and maintain constant any selected pH value.
- c) A temperature control system to keep constant the temperature during the experiment.
- d) Three flow meters to accurately maintain a constant gas flow rate for the oxygen, nitrogen, and compressed air.
- e) Piping system to transport the gases to the reactor.

### V.1.3. Methods

#### V. 1.3.1. Theoretical Parameters Affecting Hydrogen Peroxide Production

Two main chemical reactions are involved in the production of hydrogen peroxide: anodic oxidation of water:



cathodic reduction of oxygen:



From these two reactions it is obvious that current intensity, hydrogen ion concentration or pH, and oxygen concentration are determinant parameters. The solution temperature also affects the dissolved oxygen in the solution and the kinetic constant of the reaction. Since the reactions occur on the surface of the electrodes, the total available surface area of the cathode influences the hydrogen peroxide production.

a) Current Intensity. Current intensity affects the production of hydrogen peroxide in terms of current density, which is defined as the amount of amperes that flows through the anode surface area. At a certain current density value, the hydrogen peroxide production efficiency is maximum. Higher current density values will not give a better efficiency but will produce a faster consumption of the anode. Different intensity values are tested in order to determine this theoretical minimum value that gives the best efficiency with the most durability of the anode material.

b) Solution pH. Production of hydrogen peroxide is a function of the solution pH. Equation (V.2) shows that hydrogen peroxide concentration increases with decreasing the solution

pH, since the hydrogen ion concentration increases as the pH decreases. The experimental results will determine the actual pH influence.

c) Oxygen Supply. Oxygen is both quantitatively and qualitatively a limiting factor for equation (V.2). Depletion of oxygen will decrease the potential hydrogen peroxide production. So, an external source of oxygen has to be supplied. Two parameters are decisive to enhance the reaction efficiency: oxygen concentration and oxygen bubble sizes.

d) Solution Temperature. Solution temperature affects the production of hydrogen peroxide in two different ways: temperature modifies the solubility of oxygen in the solution, and it also affects the reaction kinetic constant. Oxygen solubility increases when the solution temperature decreases. The overall influence of the temperature in the oxygen solubility in the aqueous phase is tested in this experiment.

e) Cathode Surface Area. Since the hydrogen peroxide is produced on the cathode surface, larger surface areas are expected to give higher concentrations.

#### V. 1.3.2. Procedures

In order to test and demonstrate the theoretical parameters affecting the production of hydrogen peroxide, all of the described factors are tested. Figure 5.5 shows the research approach followed for this purpose. Current intensity is first tested and the most efficient value is recorded and utilized for the rest of the parameters, including pH, oxygen bubbling system, temperature and the surface area of the cathode. The following are experimental conditions:

- a) Current intensity: 0.2, 0.4, 0.6, 0.8, 1.0, 1.2 Amp.
- b) pH: 1.0, 2.0, 3.0, 4.0
- c) Oxygen rate: 2,000 cc/min
- d) Oxygen diffusion system: cylindrical pipe with 10 holes  
stone diffusers
- e) Oxygen quality: compressed air (23% O<sub>2</sub>)  
nitrogen-oxygen mixture (50% O<sub>2</sub>)  
pure oxygen (100% O<sub>2</sub>)
- f) Temperature: 12°C, 25°C (ambient), 45°C
- g) Cathode surface area: 309.67 cm<sup>2</sup> (48 sq.in),  
743.22 cm<sup>2</sup> (115.2 sq.in)  
753.54 cm<sup>2</sup> (116.8 sq.in)

## **V.2. Experimental Results**

### **V.2.1. Effect of Current Intensity**

The relationship between the voltage applied to the electrodes and the current intensity is represented in Figure 5.6. This relation shows a linear behavior within the electrolyte and, consequently, an approximately constant conductivity in the tested aqueous solution.

Figure 5.7 shows the effect of current intensity on the production of hydrogen peroxide. Starting with 0.2 Amp, hydrogen peroxide concentrations are larger when increasing the current intensity. It follows an increasing behavior until it reaches a maximum value which corresponds to a current intensity of 1 Amp. This is the limiting value for the generation of hydrogen peroxide in this experiment. Higher values will accumulate approximately the same concentrations of hydrogen peroxide or even less. However, degradation of the anode may occur, reducing its life and, therefore, increasing the overall cost of the process. When anodic decomposition occurs, small graphite particles may release into the anolyte, coloring the solution.

The generation of hydrogen peroxide over time when working with the limiting current intensity value is represented in Figure 5.8. Up to 47.83 ppm can be generated for a three hour running experiment. The effect of current intensity is actually given by the current density value which is obtained by dividing the current intensity by the surface area of the anode. For this experiment a current density value of  $6.45 \times 10^{-3}$  Amp/cm<sup>2</sup> is obtained.

### **V.2.2. Effect of Solution pH**

Solution pH has a significant influence in the production of hydrogen peroxide since the hydrogen ion concentration in the solution is a contributing factor for the hydrogen peroxide formation reaction. Figure 5.9 shows the generation of hydrogen peroxide over time for different pH values. It can be seen that pH 3.0 is the most favorable value for the generation of hydrogen peroxide, as it was reported in different studies (Sudoh et al, 1986; Chu, 1995). Almost 160 ppm hydrogen peroxide can be accumulated in a solution pH 3.0 after three hours. In a pH 1.0 solution more than a hundred ppm hydrogen peroxide can be generated over the same period of time. At pH 2.0, just 50 ppm are obtained. Finally, at higher pH values (pH  $\geq 4.0$ ), less than 40 ppm can be accumulated.

Figure 5.10 shows this pH effect on hydrogen peroxide generation. These experimental results relating the influence of solution pH on the hydrogen peroxide generation agree with Sudoh's research (Sudoh et al, 1986). Sudoh has reported that the most favorable pH for hydrogen peroxide generation is 3.0, followed by 1.0, 2.0, and 4.0 as the least beneficial value.

### **V.2.3. Effect of Oxygen Bubbling System**

Oxygen is continuously bubbled into the catholyte through a diffusion system. The oxygen inlet is placed right under the cathode in order to maximize the efficiency of the process. Figure 5.11 shows the effect of oxygen bubbles size on the production of hydrogen peroxide. Oxygen bubbles size are controlled by the use of gas diffusers. Two types of diffusers are used in this experiment: pipe diffusers and stone diffusers. Pipe diffusers are obtained by drilling ten small holes in a cylindrical pipe which is located right under the electrode in the cathodic chamber. Stone diffusers are made of a highly porous material and the compressed gas flows through these pores into the catholyte towards the cathode surface. It can be seen from Figure 5.11 that stone diffusers are more effective than pipe diffusers, since the former are able to produce smaller oxygen bubbles, which are more suitable to react on the cathode's surface to form hydrogen peroxide.

The effect of oxygen quality on hydrogen peroxide generation is shown in Figure 5.12. Three different sources of oxygen are tested. Compress air, with approximately 23% oxygen content, is bubbled into the solution. The graph shows a very small hydrogen peroxide accumulation, even after long running times. In the case of bubbling a mixture of nitrogen-oxygen (50% each), the results clearly indicate that more oxygen is transferred to the water. Pure oxygen (100%) is also bubbled into the solution and it is the most favorable situation for the hydrogen peroxide accumulation.

In conclusion, the formation rate of hydrogen peroxide is limited by the mass transport of oxygen to the cathode, the oxygen bubble size, and the oxygen content in the gas phase. Pure oxygen and the stone bubbling diffusion system are found to be the most efficient parameters for the hydrogen peroxide generation.

### **V.2.4. Effect of Solution Temperature**

Solution temperature plays an important factor on the generation of hydrogen peroxide. Figure 5.13 represents the effect of temperature on the production of hydrogen peroxide for

different times. From this graph it can be observed that at ambient temperature, 25°C, the generation of hydrogen peroxide is the more efficient than at 12° or 45°C.

Figure 5.14 represents the generation of hydrogen peroxide over time as a function of the solution temperature. Almost 200 ppm hydrogen peroxide can be accumulated after two hours at 25°C. Under the same experimental conditions, and at cooler temperatures, no more than 50 ppm hydrogen peroxide is obtained. Higher temperatures ( 45°C) are even worse and not even 10 ppm hydrogen peroxide is generated. Apparently, lower temperature inhibits the oxygen reduction reaction due to slower mass transfer process. High temperature, however, inhibits the solubility of oxygen into water. As a result an optimal temperature is necessary for the hydrogen peroxide formation reaction.

#### **V.2.5. Effect of Cathode Geometry**

Figure 5.15 represents the accumulation of hydrogen peroxide over time as a function of the cathode surface area. The plate electrode has the smallest surface area and, consequently, the lowest accumulation rate. The curve shows an increasing growth until it reaches a certain time in which the hydrogen production rate decreases to zero. The short finger cathode, with larger surface area produces higher yields, and follows the same trend, although the time to reach the steady state is larger. The long finger cathode produces the largest amount of hydrogen peroxide. Up to 273 ppm can be accumulated after 3 hours. Within this range, the production rate is linear with a value of 1.52 ppm accumulated per minute. This cathode geometry is supposed to follow the same trend as the plate and short finger. Consequently, for longer running times it will reach a certain point in which the generation rate will start to decrease.

Figure 5.16 shows the effect of the surface area of the cathode on hydrogen peroxide generation. The hydrogen peroxide production for the single plate is really low compared with the finger geometry cathodes. The largest difference is produced when looking at the hydrogen peroxide production in the short finger and comparing it with the long one.

#### **V.2.6. Current Efficiency for Hydrogen Peroxide**

Table 5.2 shows the calculated values for the current efficiency. The experimental conditions are as follows: 1 Amp; solution pH 3.0; stone diffusers; 100% oxygen; 2,000 cc/min oxygen flow rate; temperature 25°C; long finger cathode with a total available surface area of 753.54 sq. cm.

Figure 5.17 shows that the current efficiency for the formation of hydrogen peroxide is 81% after the first 5 minutes, but decreases rapidly as hydrogen peroxide accumulates in the acidic solution. Sudoh (Sudoh et al, 1986) obtained a maximum current efficiency for the hydrogen peroxide formation of 85% in a solution pH 3.0.

Table 5.2. Current efficiency for the hydrogen peroxide generation.

<b>Time (min)</b>	<b>Hydrogen peroxide (ppm)</b>	<b>Current efficiency (%)</b>
5	9.54	81.25
10	18.94	80.62
15	28.00	79.47
30	53.53	75.96
60	103.46	73.41
90	149.03	70.49
120	195.05	69.19
150	233.46	66.26
180	273.46	64.68

### **V.2.7. Hydrogen Peroxide Stability**

From a theoretical point of view, the tendency of absolutely pure hydrogen peroxide to decompose into water and oxygen is negligible. This appears to be true even if the pure material is in aqueous solution, provided that the water of the solution is absolutely pure. However, in practice, numerous agents or conditions tend to initiate or accelerate decomposition. Thus, a very slight trace of dissolved impurity such as ferric ions or other metallic ions exert a marked catalytic decomposition effect.

Figure 5.18 shows the degradation rate of commercial hydrogen peroxide under different acidic pH values. Within the acidic pH range, the degradation of hydrogen peroxide is almost negligible. However, in the alkaline pH region, the hydrogen peroxide disappears after 10 hours.

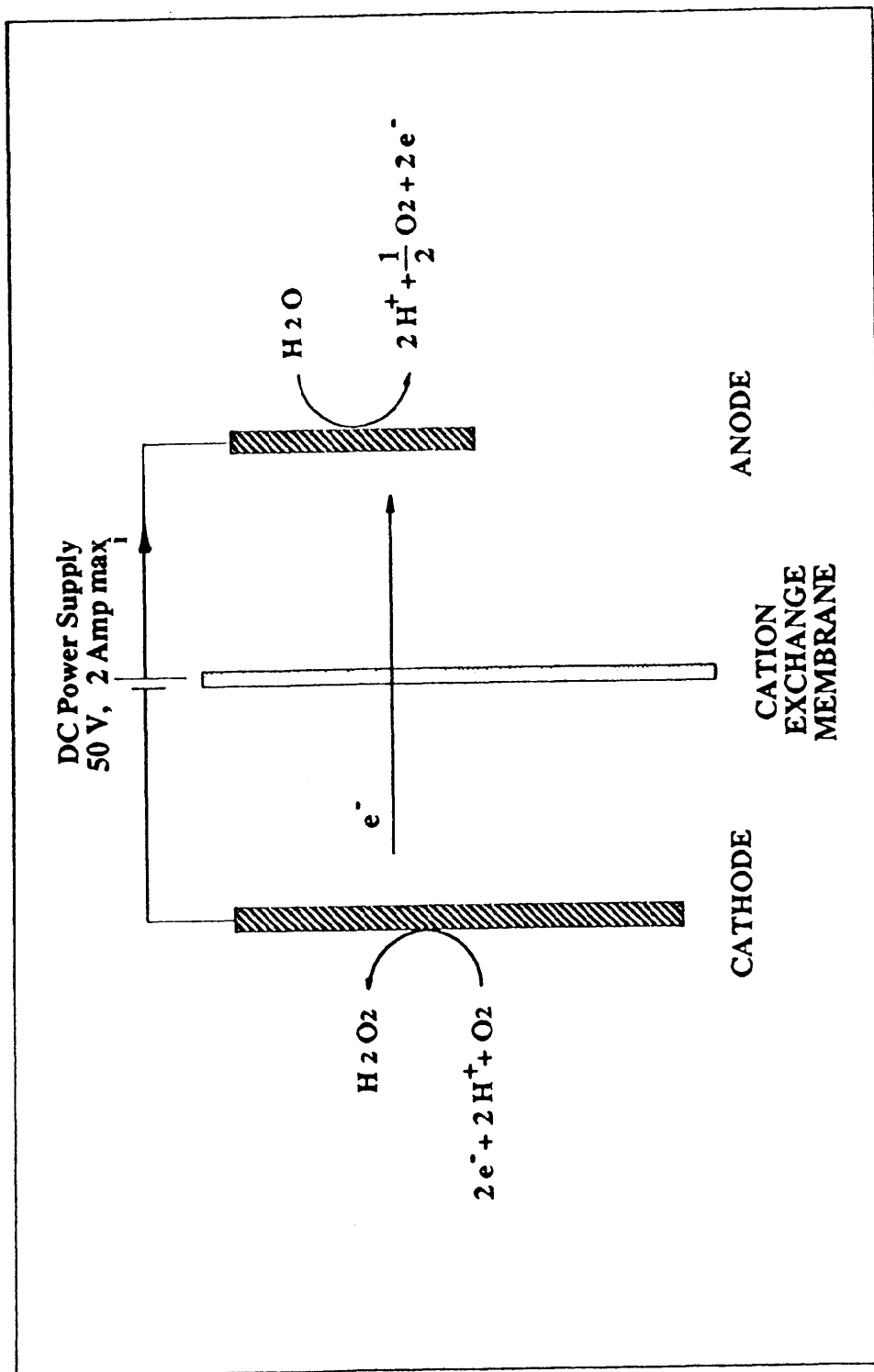


Figure 5.2 Schematic of the electrolysis cell for the production of hydrogen peroxide

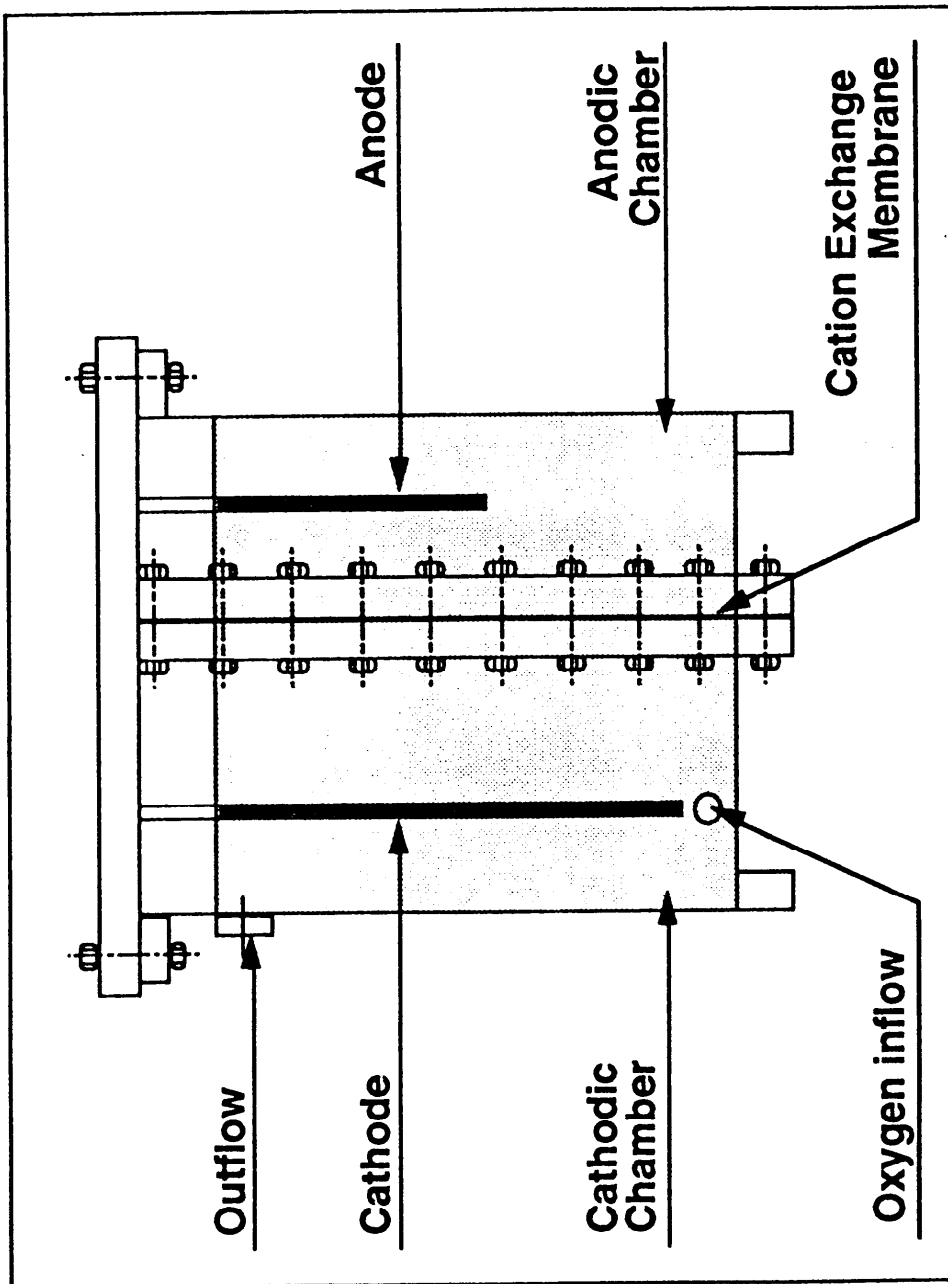


Figure 5.1 Schematic of the reactor configuration.

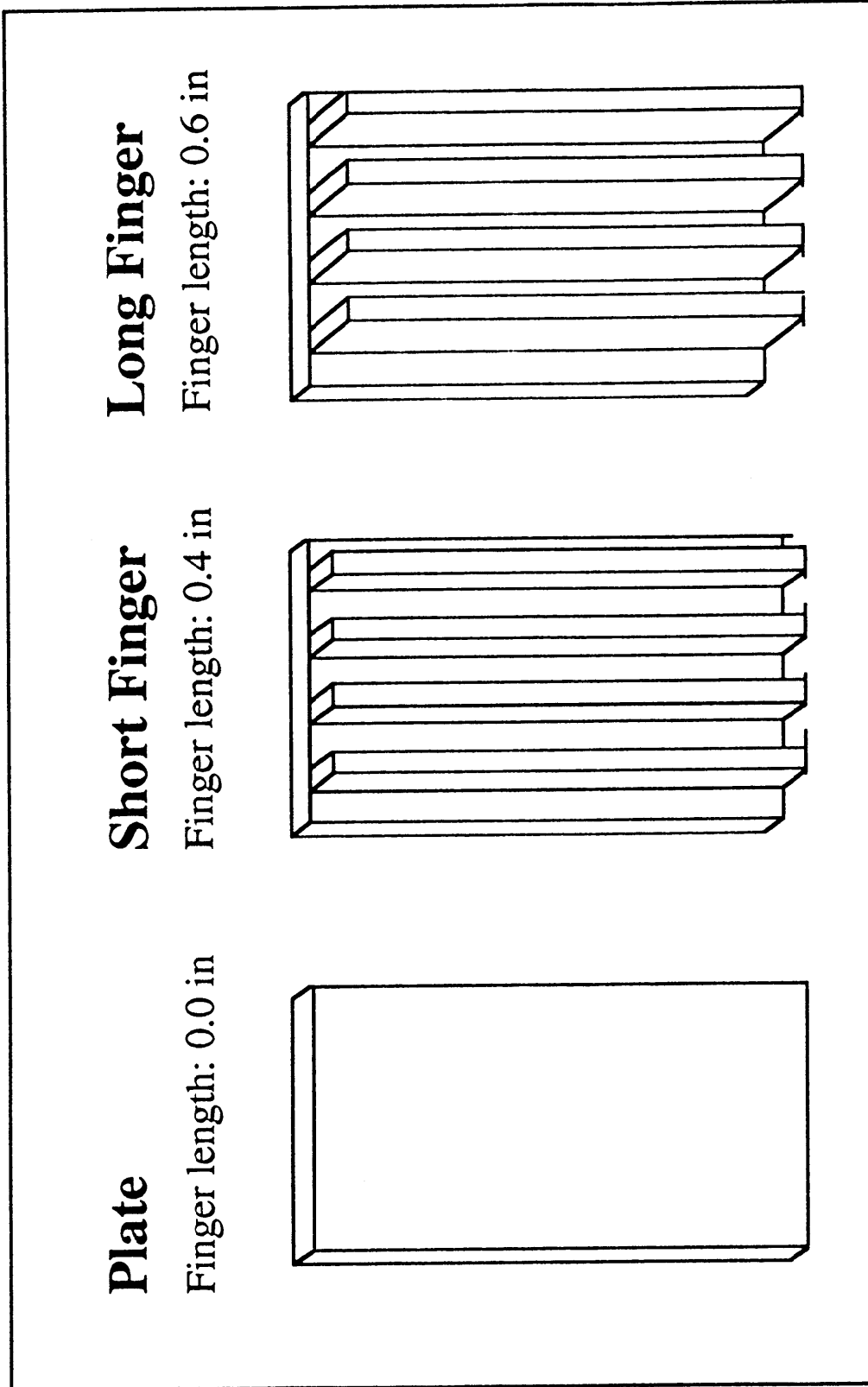


Figure 5.3 Schematic of three cathodes geometry

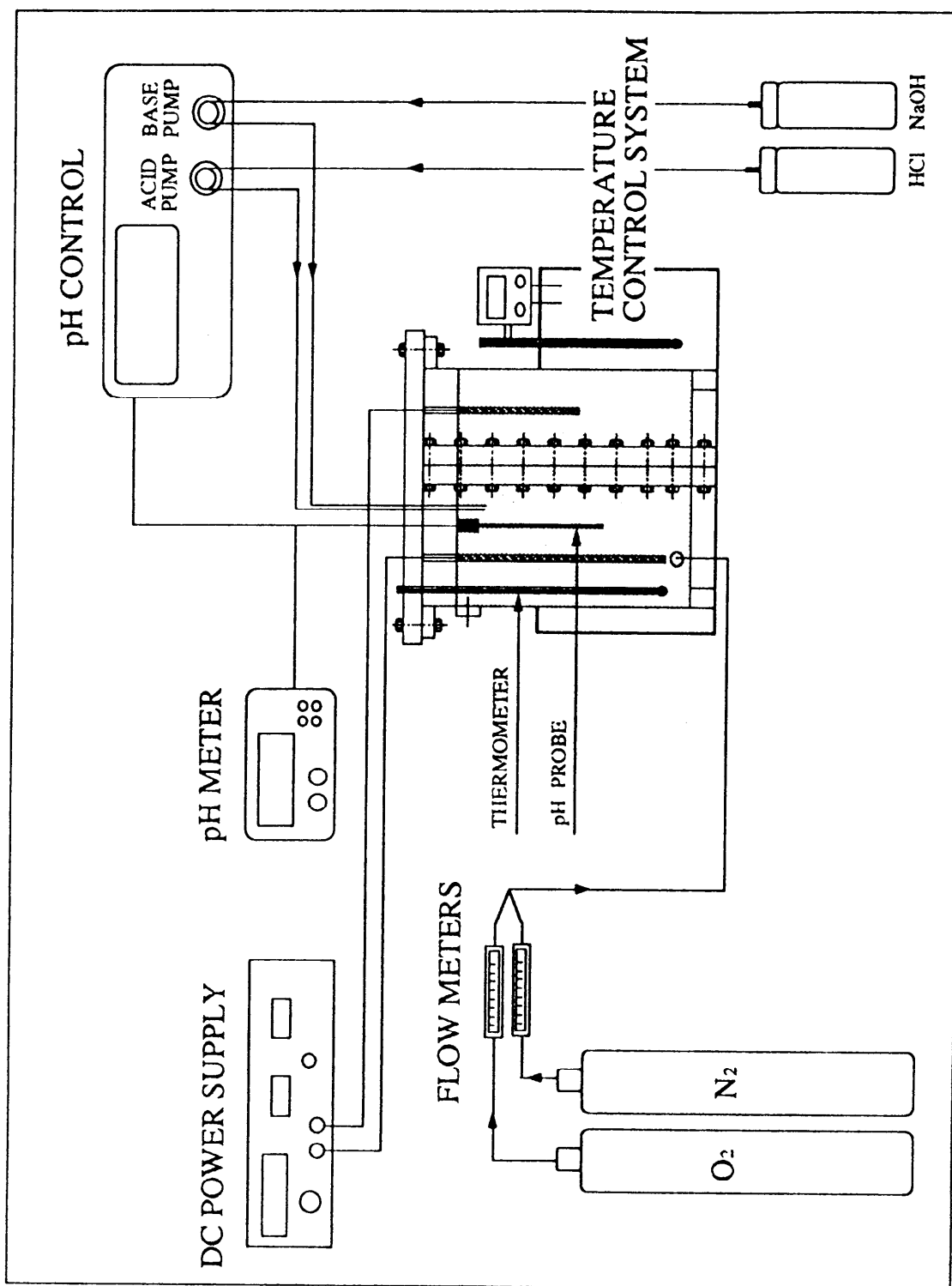


Figure 5.4 Schematic of the laboratory setup configuration

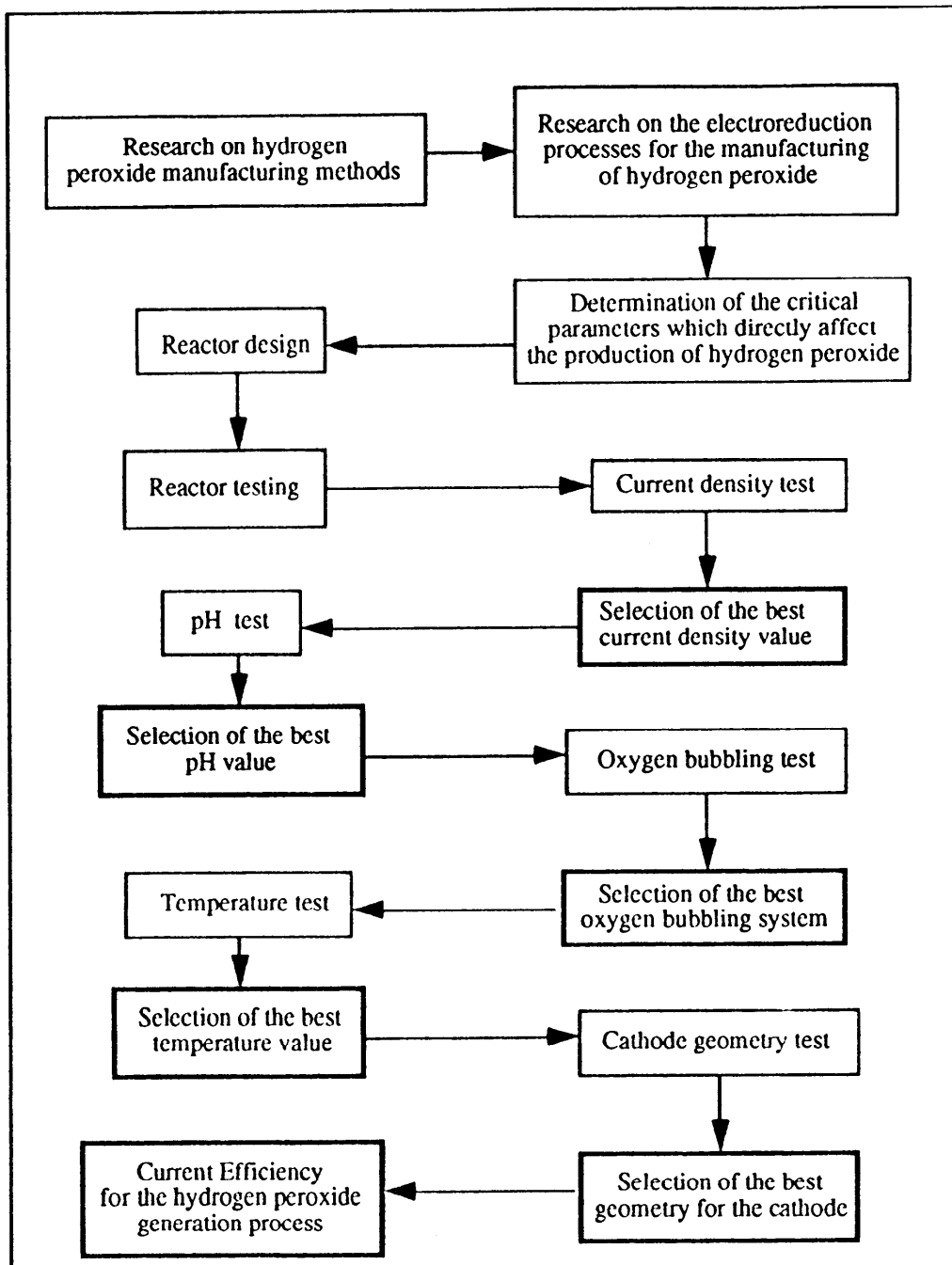
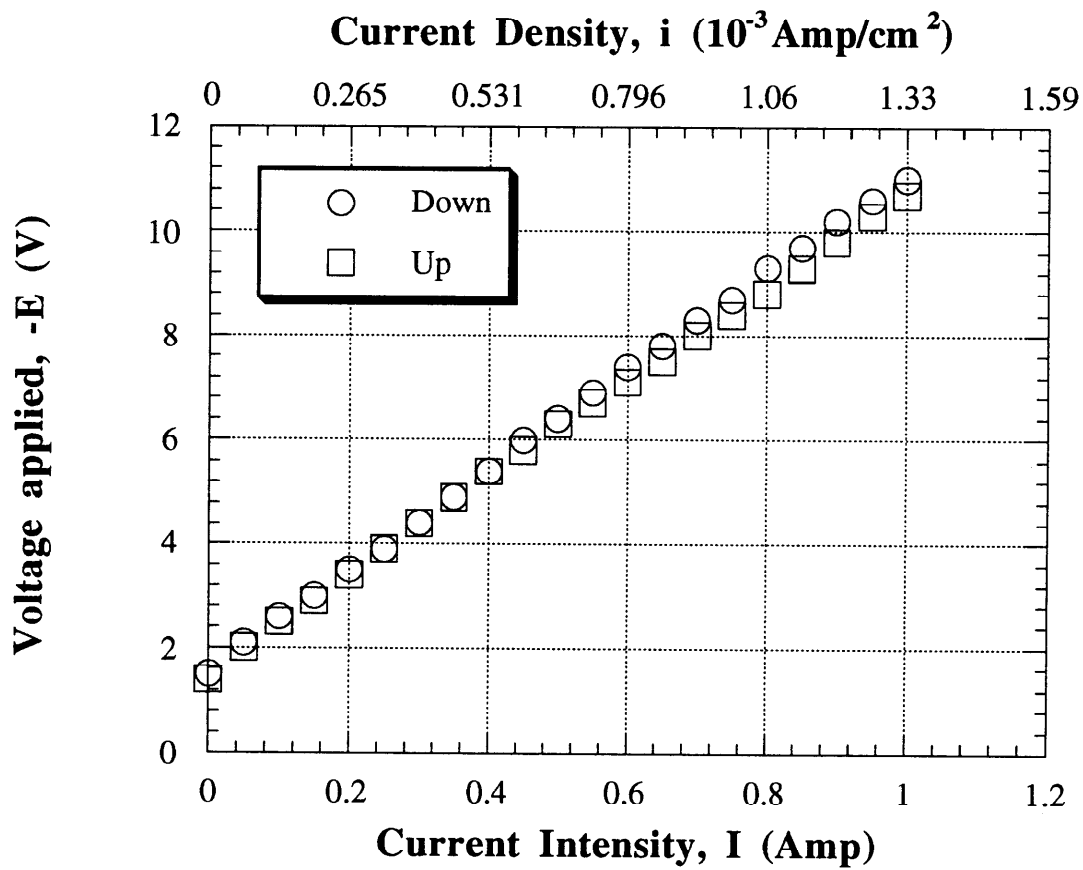
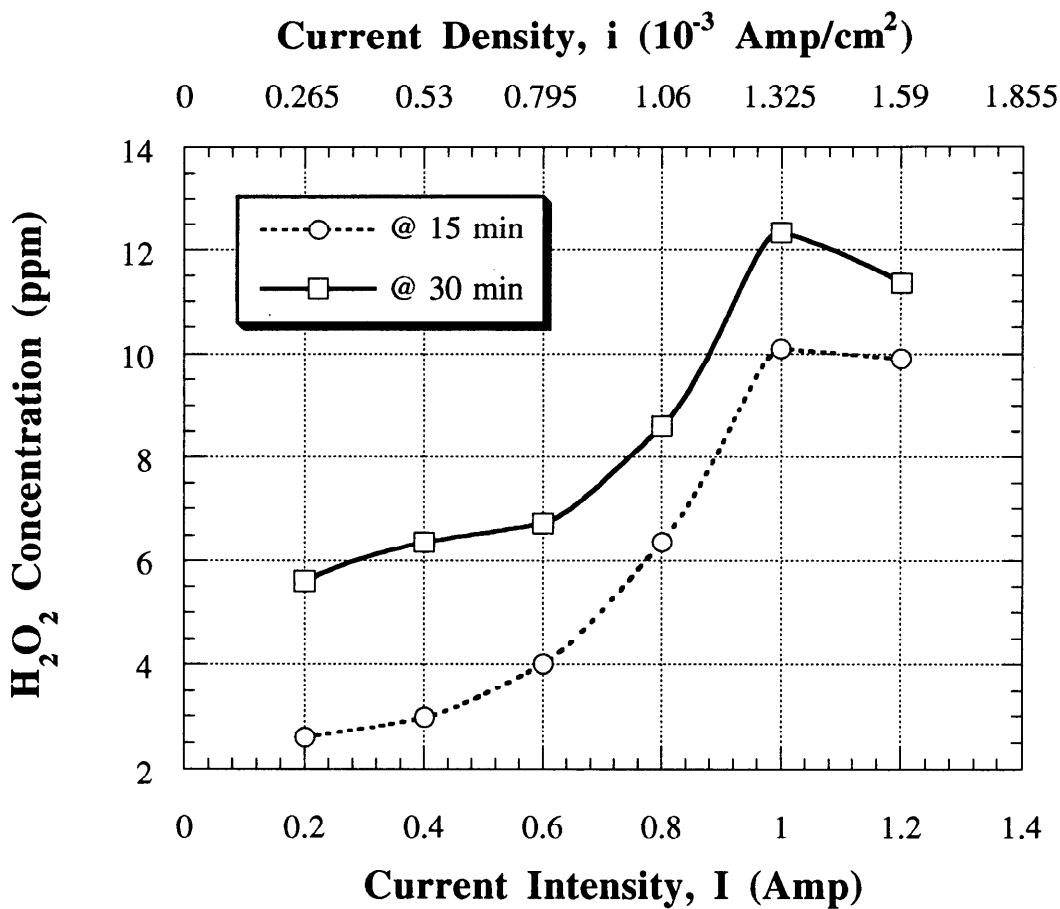


Figure 5.5 Flow diagram for the research approach



**Figure 5.6** The relationship between the applied voltage and the current intensity in a 0.05 M NaClO<sub>4</sub> ionic strength solution.



**Figure 5.7** The effect of current intensity on hydrogen peroxide concentration. Working conditions: solution ionic strength: 0.05 M NaClO<sub>4</sub>; solution pH 2.0; pipe diffusion system; oxygen flow rate: 2,000 cc/min; 100% oxygen quality; 25°C solution temperature; 753.54 sq.cm cathode's surface area.

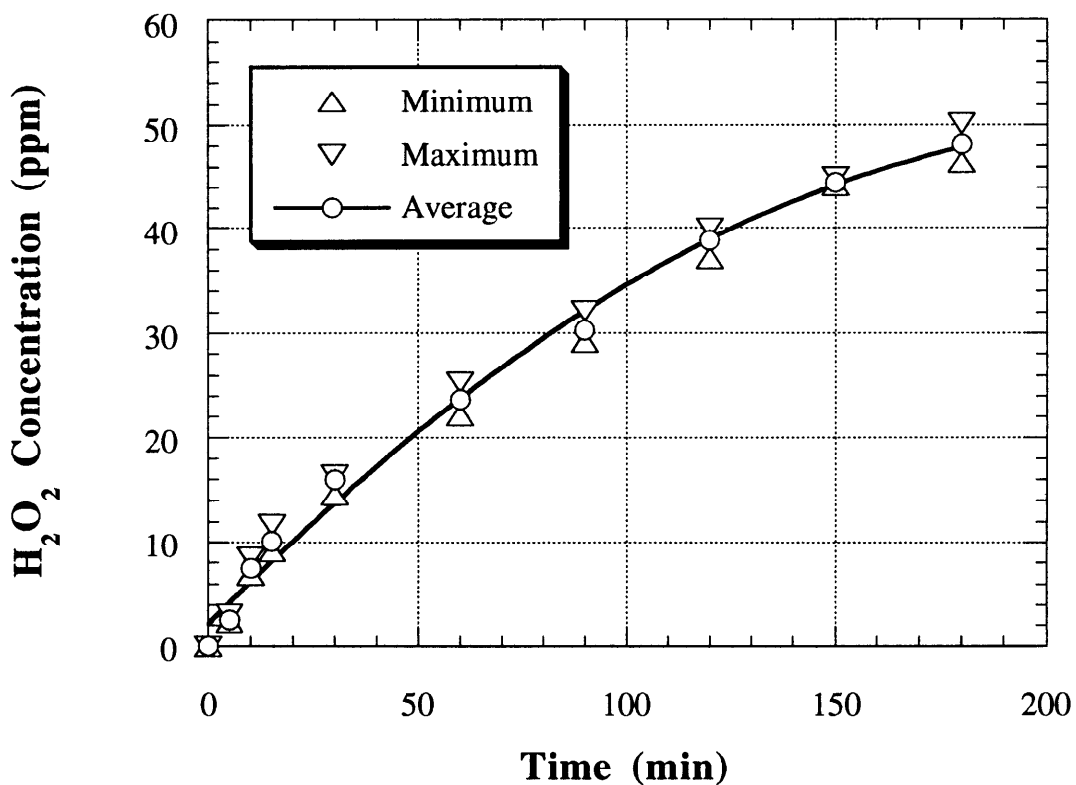


**Figure 5.8** The generation of hydrogen peroxide over time for a constant current intensity of 1 Amp. Working conditions: solution ionic strength: 0.05 M NaClO<sub>2</sub>; solution pH 2.0; pipe diffusion system; oxygen flow rate: 2,000 cc/min; 100% oxygen quality; 25°C solution temperature; 753.54 sq.cm cathode's surface area.

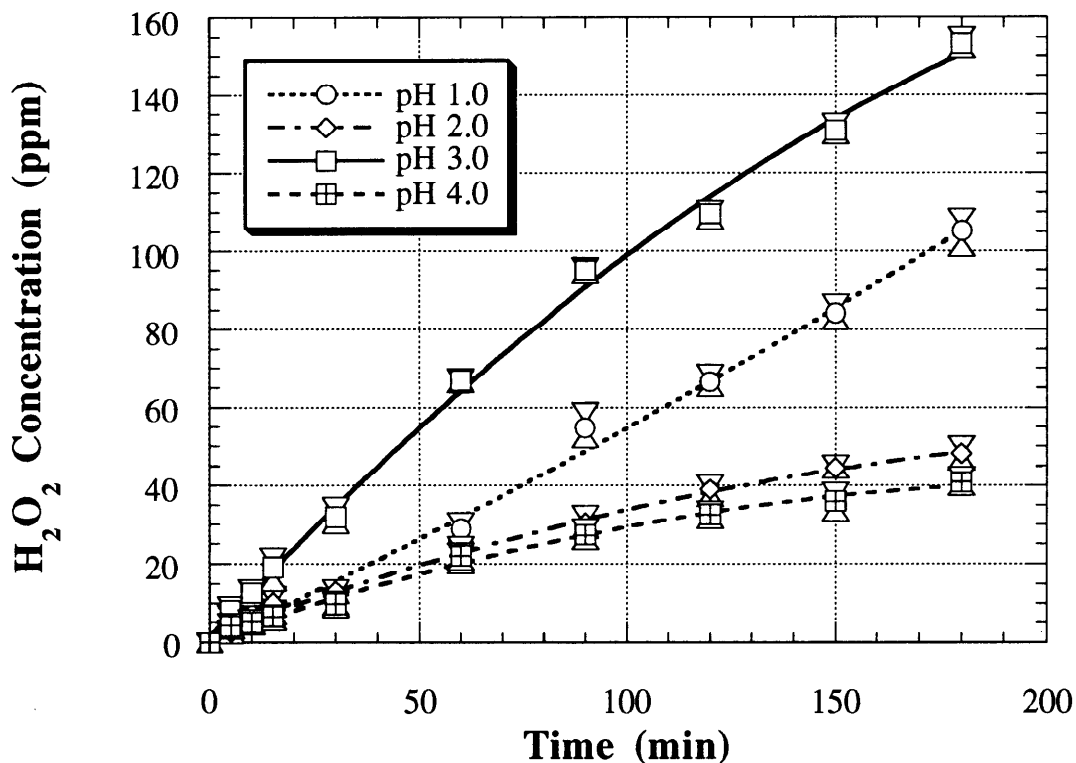


**Figure 5.9** The generation of hydrogen peroxide over time for different pH values. Working conditions: solution ionic strength: 0.05M NaClO<sub>4</sub>; current intensity 1 Amp; pipe diffusion system; oxygen flow rate: 2,000 cc/min; 100% oxygen quality; 25°C solution temperature; 753.54 sq.cm cathode's surface area.

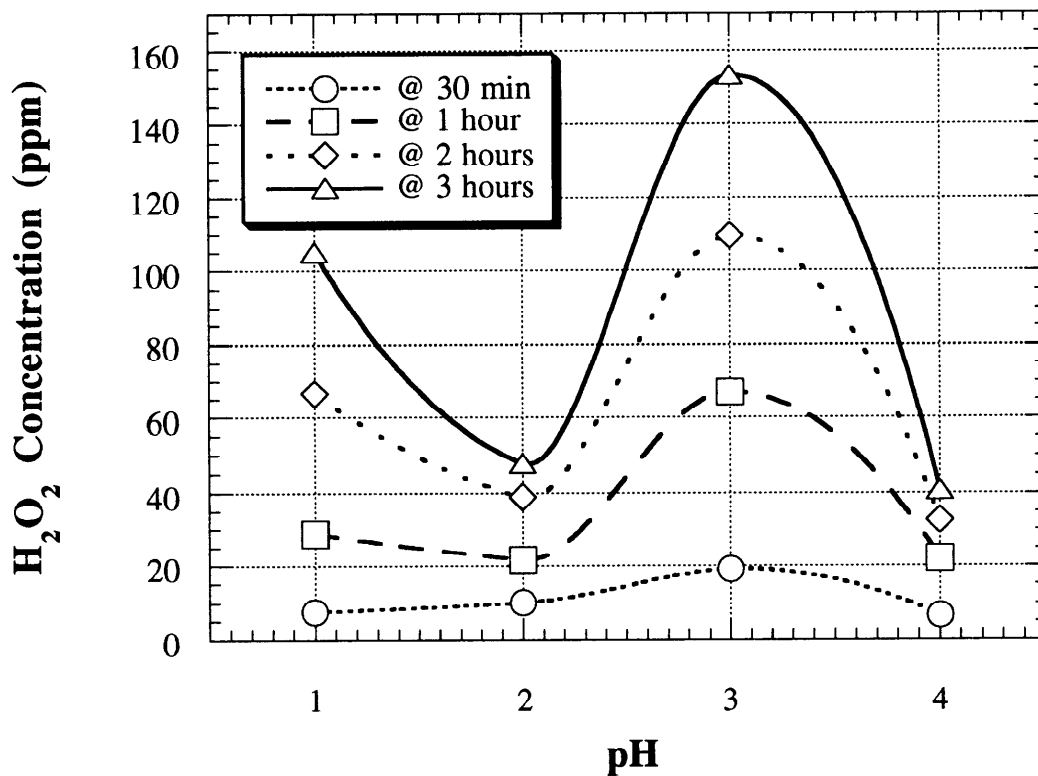


**Figure 5.10** The effect of pH on hydrogen peroxide concentration.  
**Working conditions:** solution ionic strength: 0.05 M NaClO<sub>4</sub>;  
 current intensity 1 Amp; pipe diffusion system; oxygen flow  
 rate: 2,000 cc/min; 100% oxygen quality; 25°C solution  
 temperature; 753.54 sq.cm cathode's surface area.

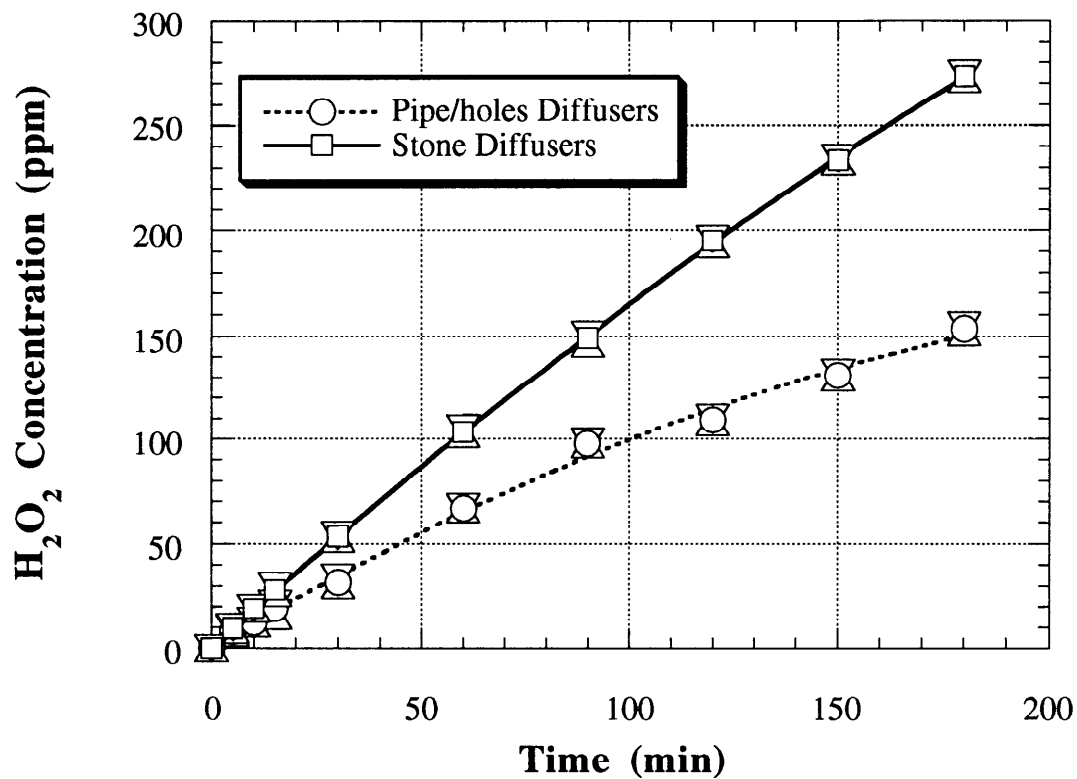


**Figure 5.11** The effect of oxygen bubbles' size on hydrogen peroxide generation. Working conditions: solution ionic strength: 0.05 M NaClO<sub>4</sub>; current intensity 1 Amp; solution pH 3.0; oxygen flow rate: 2,000 cc/min; 100% oxygen quality; 25°C solution temperature; 753.54 sq.cm cathode's surface area.

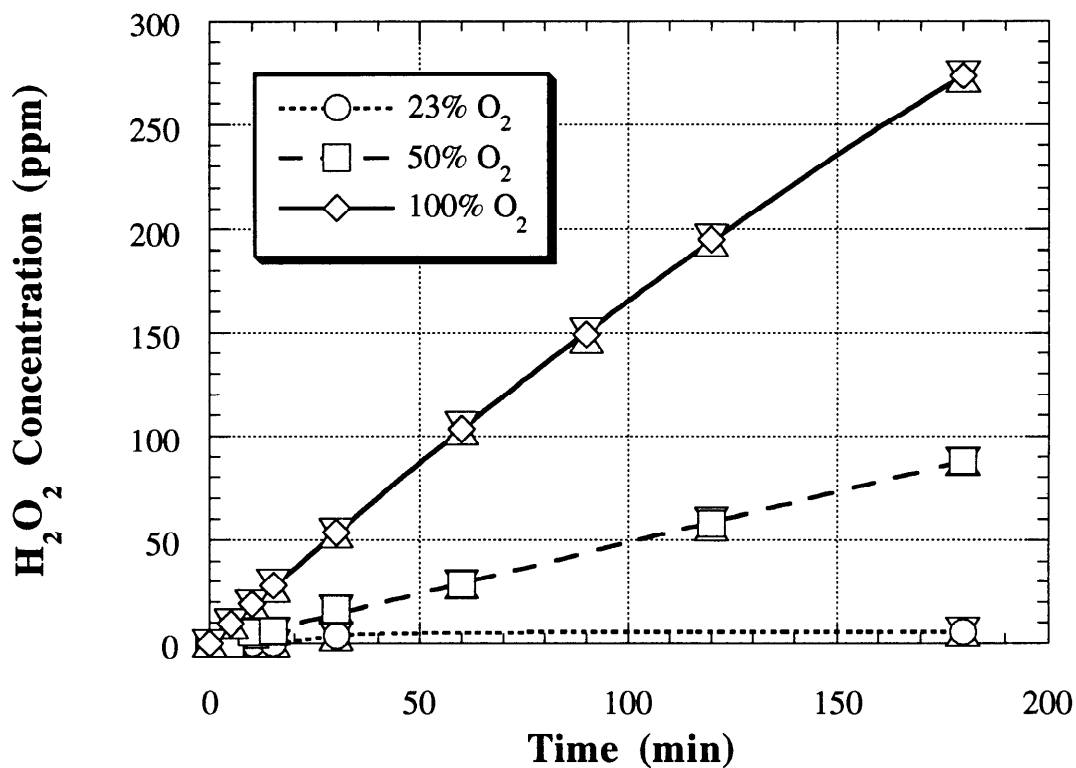


**Figure 5.12** The effect of oxygen quality on hydrogen peroxide concentration. Working conditions: solution ionic strength: 0.05 M NaClO<sub>4</sub>; current intensity 1 Amp; solution pH 3.0; oxygen flow rate: 2,000 cc/min; stone diffusion system; 25°C solution temperature; 753.54 sq.cm cathode's surface area.

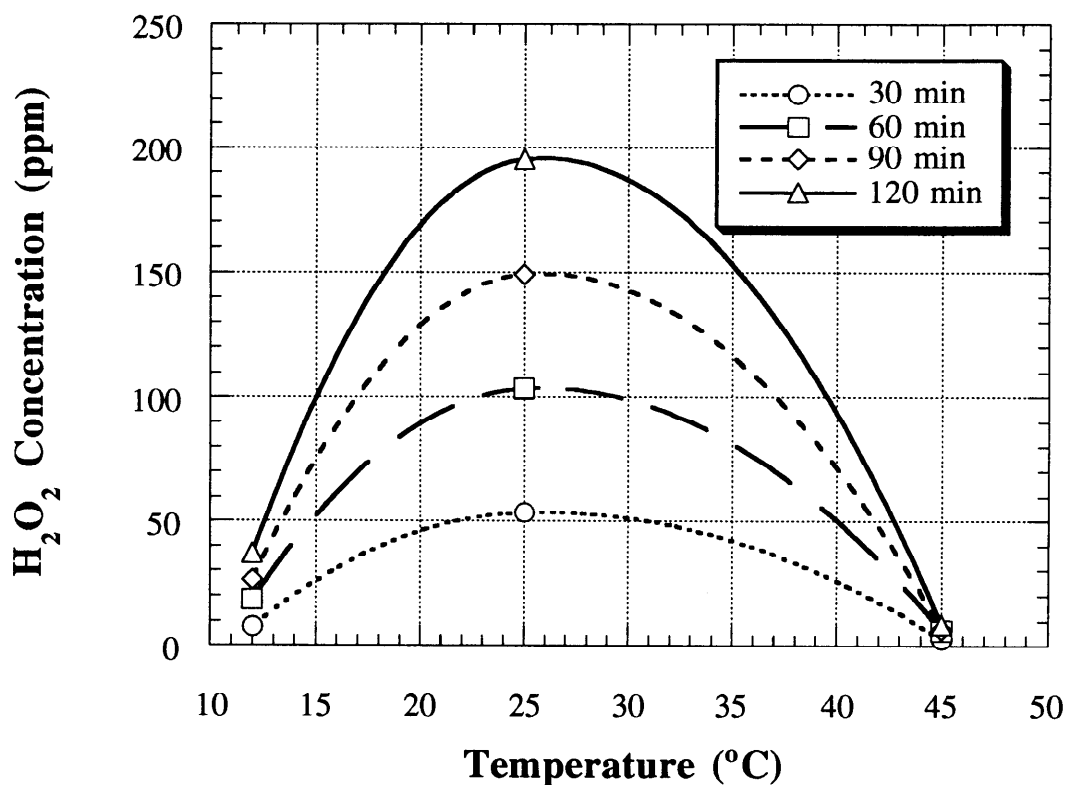


**Figure 5.13** The effect of solution temperature on hydrogen peroxide concentration. Working conditions: solution ionic strength: 0.05 M NaClO<sub>4</sub>; current intensity 1 Amp; solution pH 3.0; oxygen flow rate: 2,000 cc/min; pipe diffusion system; 100% oxygen quality; 753.54 sq.cm cathode's surface area.

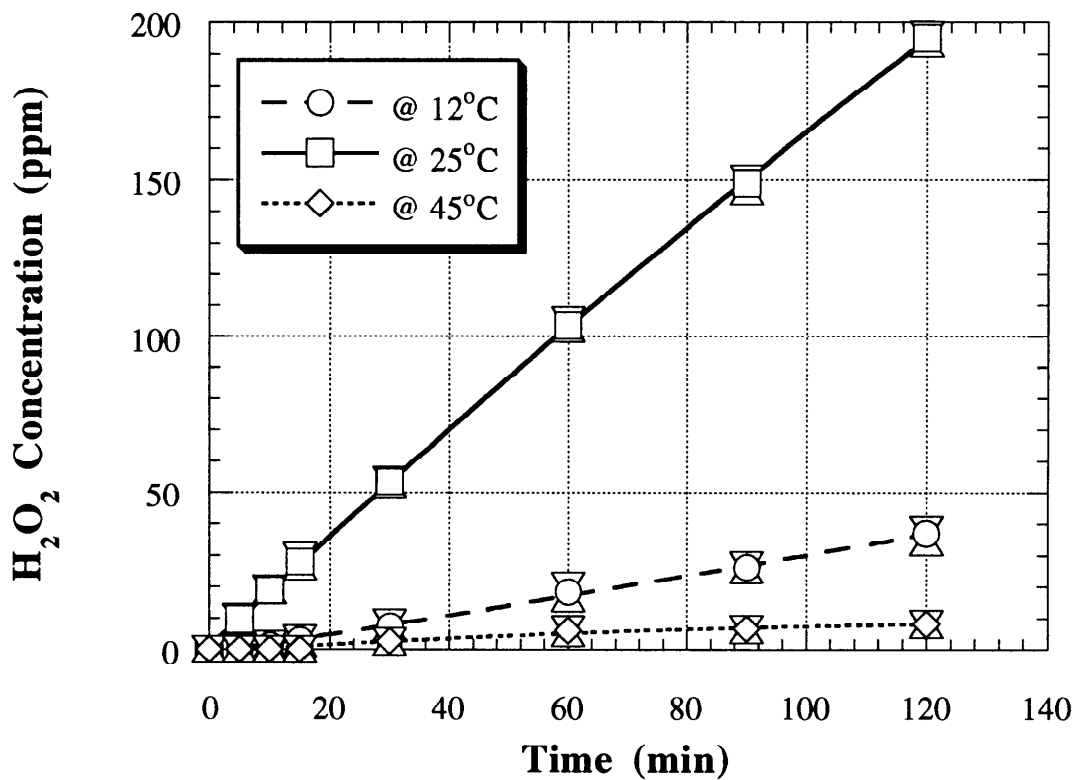


**Figure 5.14** The generation of hydrogen peroxide concentration over time as a function of solution temperature. Working conditions: solution ionic strength: 0.05 M NaClO<sub>4</sub>; current intensity 1 Amp; solution pH 3.0; oxygen flow rate: 2,000 cc/min; pipe diffusion system; 100% oxygen quality; 753.54 sq.cm cathode's surface area.

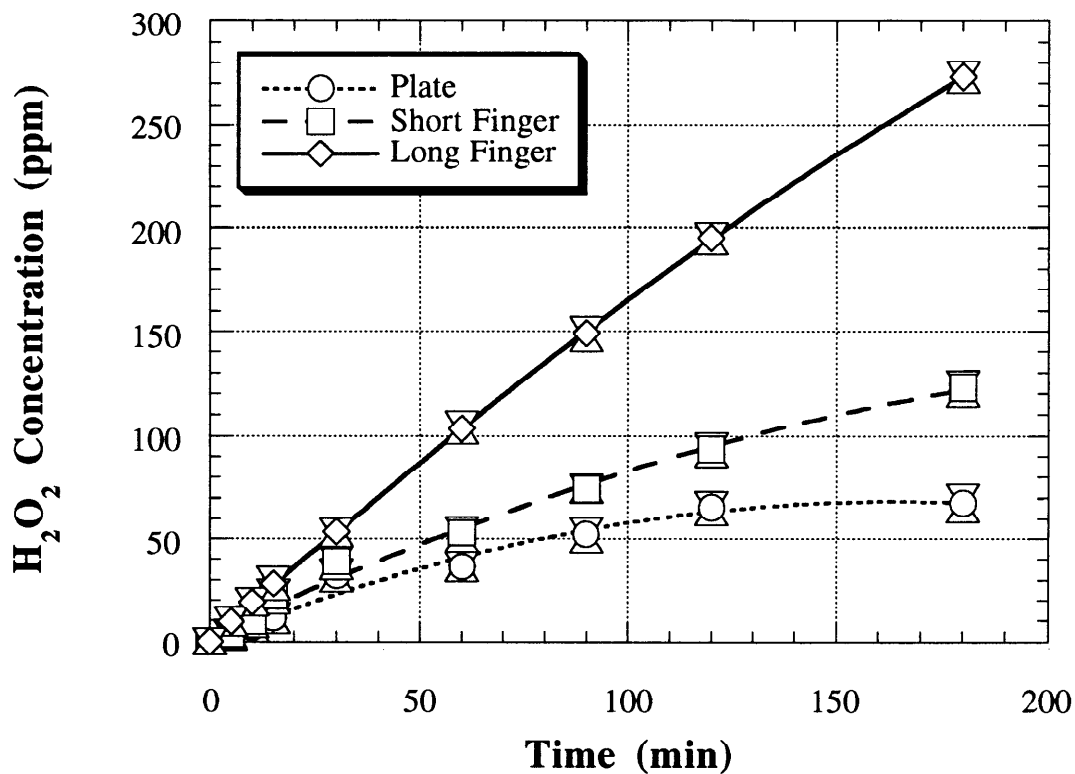


**Figure 5.15** The generation of hydrogen peroxide over time as a function of the cathode's surface area. Working conditions: solution ionic strength: 0.05 M NaClO<sub>4</sub>; current intensity 1 Amp; solution pH 3.0; oxygen flow rate: 2,000 cc/min; pipe diffusion system; 100% oxygen quality; 25°C solution temperature.

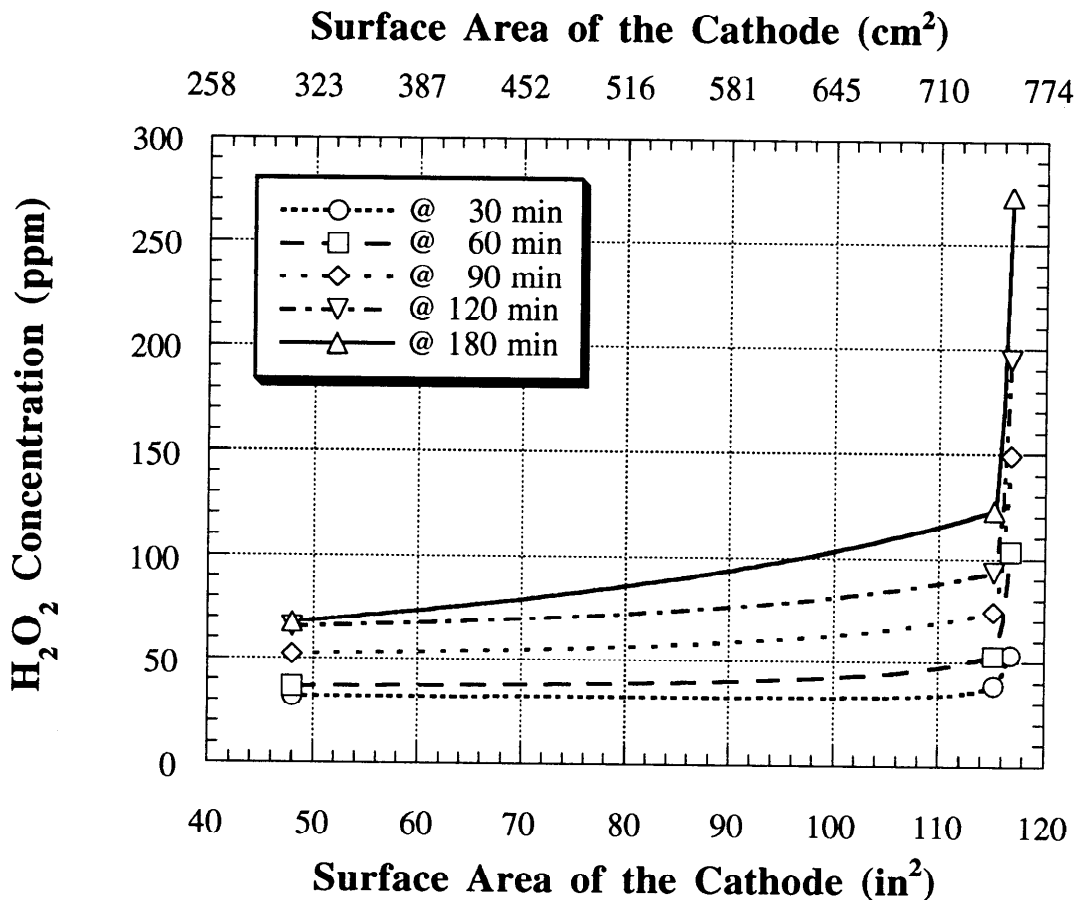


**Figure 5.16** The effect of cathode's surface area on hydrogen peroxide concentration. Working conditions: solution ionic strength: 0.05 M NaClO<sub>4</sub>; current intensity 1 Amp; solution pH 3.0; oxygen flow rate: 2,000 cc/min; pipe diffusion system; 100% oxygen quality; 25°C solution temperature.

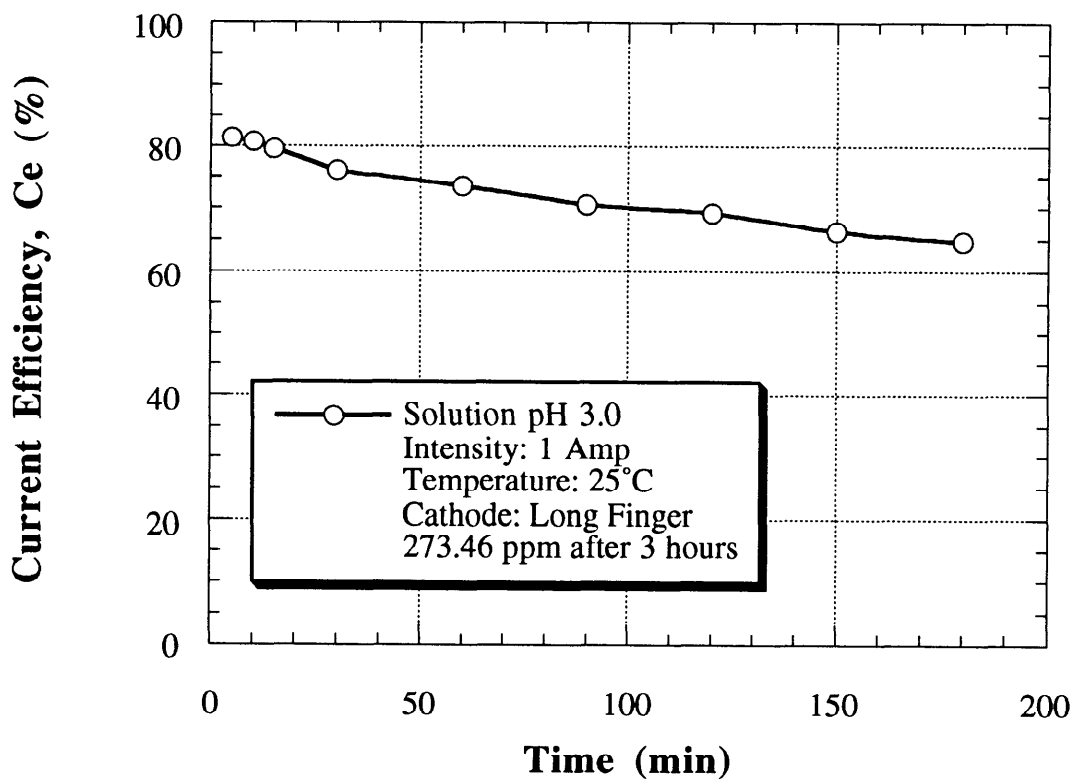


**Figure 5.17 Current Efficiency for the hydrogen peroxide generation. Working conditions: solution ionic strength: 0.05 M NaClO<sub>4</sub>; current intensity 1 Amp; solution pH 3.0; oxygen flow rate: 2,000 cc/min; stone diffusion system; 100% oxygen quality; 25°C solution temperature; 753.54 sq.cm cathode's surface area.**

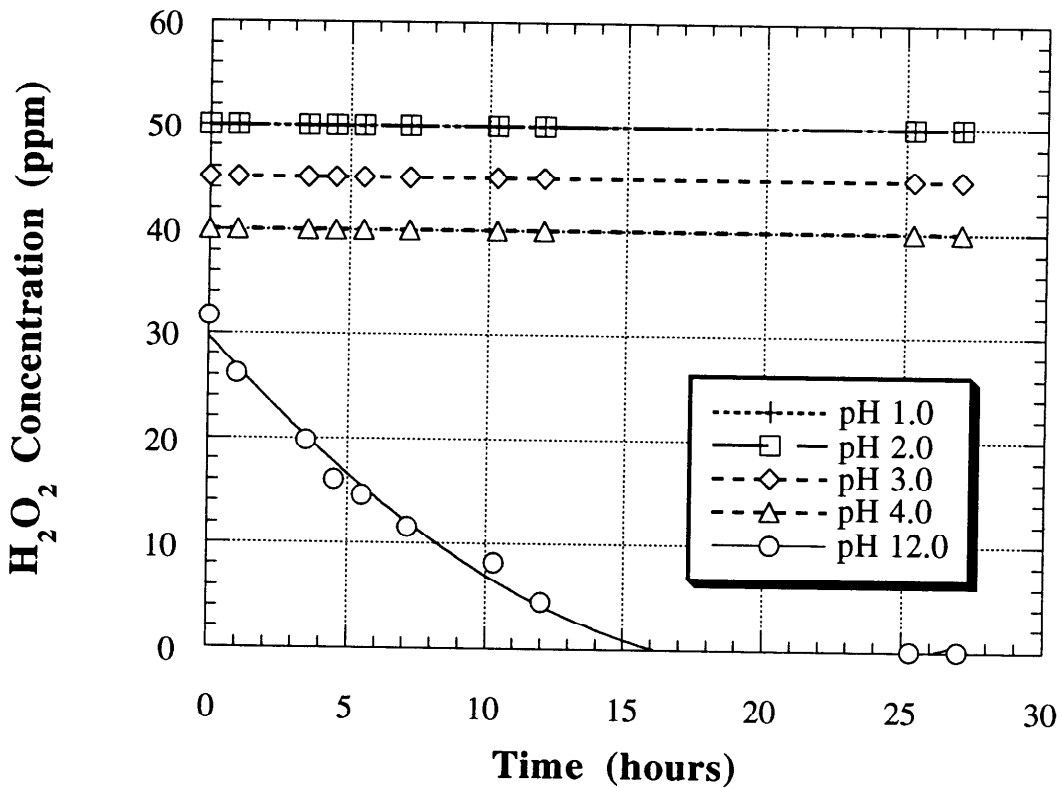


**Figure 5.18 Hydrogen peroxide stability over time as a function of solution pH.**

## **VI. Future Work**

### **VI.1. Adsorption of Selected Organic Compounds on Soils**

The adsorption characteristics of other organic compounds will be determined using batch experiments. A given amount of soil received from contaminated sites will be mixed with a solution containing the single or mixed selected organic compounds ( chlorinated compounds and PAHs ). Because the adsorption of some chemical contaminants are associated with pH, adsorption characteristics will be measured as a function of pH. Tentatively, the pH will vary from 4 to 10. Other influential factors, such as soil to solution ratio, soil organic content that can affect the adsorption of selected organic compounds will also be studied.

### **VI.2. Electra-Osmosis Experiments**

The movement of selected organic compounds in aquifer under the influence of an imposed electric field will be studied in the laboratory. Electra-Osmosis experiments will be conducted to study the effect on the movement of selected organic compounds ( chlorinated compounds and PAHs) in selected soil samples.

### **VI.3. Electra-Fenton Experiments**

A given amount of the selected organic compounds (chlorinated compounds and PAHs) will be spiked into the solution in the electro-Fenton reactor. At a pre-selected reaction time, the concentration of the selected organic compounds will be determined. The reaction intermediates will be identified using GC/MS and HPLC/UV spectrophotometer. The current efficiency will also be determined.

## VII. REFERENCES

1. Acar, Y. B.; and Alshwabkeh, A. N. (1993). Principles of Electrokinetic Remediation. *Environmental Science and Technology*, 27, 2638-2647.
2. Casagrande, L. (1949). Electroosmosis in Soils. *Geotechnique*, 1, 159.
3. Chu, C.S. (1995). The Electrochemical Oxidation of Recalcitrant Organic Compounds, Doctor of Philosophy Thesis, Civil and Environmental Engineering Department, University of Delaware, Newark.
4. Ferris A.P. and Jepson W.B. (1975) The exchange capacities of kaolinite and the preparation of homoionic clays. *J. Colloid and Interface Sci.* 51, 245-259.
5. Hamed, J.; Acar, Y. B.; and Gale, R. J. (1991). Pb(II) Removal from Kaolinite by Electrokinetics. *Journal of Geotechnical Engineering Division, ASCE*, 117, 241-271.
6. Holmes-Farley, S.R. (1988) Binding of phenols to aluminum oxide surfaces. I. phenols with a single hydroxy group. *Langmuir* 4, 768-774.
7. Kezdi, A. (1980). *Soil Testing*. Elsevier Scientific, New York, N. Y.
8. Lee L.T., Rahbari J., Lecourtier J. and Chauveteau G. (1991) Adsorption of polyacrylamides on the different faces of kaolinites. *J. Colloid Interface Sci.* 147, 351-357.
9. Lu F., Salaita G.N., Laguren-Davidson L., Stem D.A., Welner E., Frank D.G., Batina N., Zapien D.C., Walton N. and Hubbard A.T. (1988) Characterization of hydroquinone and related compounds adsorbed at pt( 111) from aqueous solutions: electron energy-loss spectroscopy, Aufer spectroscopy, low-energy electron diffraction, and cyclic voltammetry. *Langmuir* 4, 637-646.
10. McBride M.B. and Wesselink L.G. (1988) Chemisorption of Catechol on gibbsite, boehmite, and noncrystalline alumina surfaces. *Environ. Sci. Technol.* 22, 703-708.
11. Pamukcu, S.; and Khan, L. I. (1989). Validity of Electra-Osmosis for Soil Decontamination. *Environmental Engineering*, 10, 563-570.

12. Pefferkorn, E., Nabzar L. and Varoqui R. (1987) Polyacrylamide na-kaolinite interactions: effect of electrolyte concentration on polymer adsorption. *Colloid Polymer Sci.* 265, 889-896.
13. Sims, J.T. and Heckendorn, S.E. (1991). *Methods of Soil Analysis*, University of Delaware, Agricultural-Experimental Station Cooperative Extension, Newark.
14. Sudoh, M., Kodera, T., Sakai, K., Zhang, J. Q., and Koide, K. (1986). Oxidative Degradation of Aqueous Phenol Effluent with Electrogenerated Fenton's Reagent, *J. Chemical Engineering Japan*, 19, 6-15.

## VIII. APPENDIX ANALYTICAL METHODS

### A. Soil Characterization

#### A. 1. Composition Analysis

The composition of site clay material was analyzed by the sedimentation (hydrometer) method. The procedures were as follows:

- a) Grind soil samples with mortar and pestle and sieve to make sure that all the diameters of the soil particles are less than 2 mm.
- b) Take 50 gram of the ground soil sample and add 100 mL of 5% sodium hexametaphosphate.
- c) Transfer the suspension to a sedimentation cylinder, insert a plunger and mix the contents thoroughly.
- d) About 15 seconds after mixing the suspension, lower the hydrometer into suspension, and after 40 seconds, read the scale at the top of the meniscus.
- e) Record the hydrometer value.
- f) Record temperature of the sample and blank at the 40 seconds time mark. From these values, the percentage of sand can be calculated.
- g) After 2 hours of standing lower the hydrometer into the sedimentation cylinder and record the hydrometer value, then record the temperature of sample and blank. From these values, the percentage of clay can be calculated.

The equations for the calculation of the soil composition are as follows:

$$\% \text{ Sand} = 100 - \left[ \frac{100 \times (\text{hydrometer reading at 40 seconds})}{(\text{Corrected weight of Soil})} \right]$$

$$\% \text{ Clay} = \frac{100 \times (\text{hydrometer reading at 2 hours})}{(\text{Corrected weight of Soil})}$$

$$\% \text{ Silt} = 100 - (\% \text{ Sand} + \% \text{ Clay})$$

where: Corrected Weight of Soil =  $\frac{\text{oven dry weight of subsample} \times 50\text{g}}{\text{Air - dried weight of subsample}}$

## A.2. Soil pH

The pH measurement was made in 0.01 M CaCl<sub>2</sub> solution. The samples were air dried and sieved through 2 mm sieve to remove the coarse soil fraction. Weigh 10 gram of the pretreated soil sample and mix with 10 mL of 0.01 M CaCl<sub>2</sub>. Mix thoroughly and let the sample stand for at least 1 hour. Record the pH value by using a pH meter.

## A.3. Soil Organic Matter

The soil organic matter was determined by the loss of weight on ignition (L. O. I.) method.

Take 1 cm<sup>3</sup> of air dried and sieved through 2mm sieve soil sample and place it into a 30 mL beaker. Dry the soil sample at 105 °C for two hours. Record the weight of soil sample plus beaker with an accuracy of +0.001 g. Heat the sample in oven at 360°C for two hours. Cool the sample to 105 °C and maintain at this temperature until weighing. Weigh the beaker with the ash in a draft-free environment to ±0.001 g.

$$\text{O.M. (\%)} = \frac{(W_{bs} - W_b) - (W_{ba} - W_b)}{W_{bs} - W_b} \times 100$$

where:  $W_b$  = weight of beaker,  
 $W_{bs}$  = weight of beaker plus soil before ashing,  
 $W_{ba}$  = weight of beaker plus ashed soil.

## A.4. Soil Effective Cation Exchange Capacity

a) Determination of the exchangeable cations

Weigh 10 g of soil sample into a 100 mL polyethylene cup and add 50 mL of 1 N ammonium acetate (NH<sub>4</sub>OAc) to the cup as a buffer solution to maintain the solution pH at 7.0. Shake the cup for 30 minutes. Filtrate the suspension with No. 40 filter paper (Whatman) and add 25 ml of 1 N NH<sub>4</sub>OAc again to wash the filter paper. Collect the filtrate and determine the K, Ca and Mg concentrations by atomic absorption spectrophotometer.

b) Determination of exchangeable acidity

Weigh 10 g of soil sample into a 125 mL Erlenmeyer flask, add 25 ml of 1 N KCl solution and mix well. Filtrate the suspension into a 300 mL Erlenmeyer flask. Add 4 drops of phenolphthalein indicator to the KCl solution. Titrate the KCl solution with the standard 0.01 N NaOH. At the end point of titration, record the volume of NaOH used. Get the exchangeable acidity in (meq/100g).

c) Effective cation exchangeable capacity (ECEC)

The sum of the concentrations of exchangeable K, Ca, Mg and the exchangeable acidity is the effective cation exchangeable capacity (ECEC).

### **A5. Moisture Content**

Measure the empty aluminum plate and record the weight first. Weight 1 g of soil on the aluminum plate. Measure and record the weight of plate with soil and record it. Put the soil sample in oven at 105 °C for 24 hours to get rid of soil moisture. Take these samples from the oven to the desiccator and for cool. Measure the weight of the dried soil.

The moisture content is for calculated as the following:

$$M(\%) = \frac{W_{\text{wet soil}} - W_{\text{dry soil}}}{W_{\text{wet soil}} - W_{\text{plate}}} \times 100$$

where: M(%) = moisture content, percentage by weight

$W_{\text{wet soil}}$  = weight of original soil sample + aluminum plate

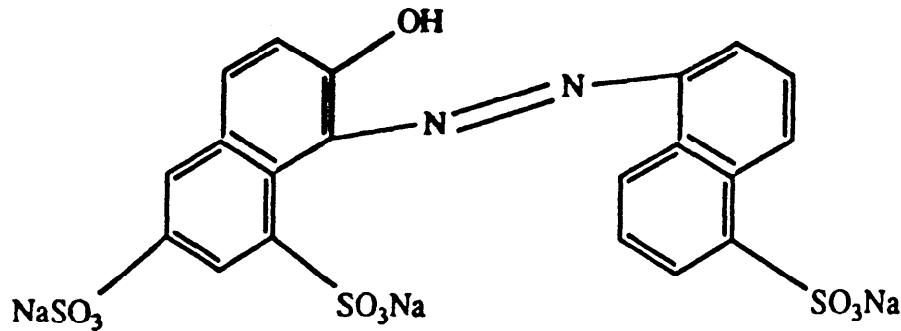
$W_{\text{dry soil}}$  = weight of the ashed soil + aluminum plate

$W_{\text{plate}}$  = weight of the aluminum plate

### **A.6. Specific Surface Area**

The dye adsorption method (Smith and Coachley, 1983) was selected to determine the specific surface area of soils in this study. A commercially available dye, coccine acid red #18 (Aldrich Chemical Company, Inc.), was utilized as an adsorbate. This dye has a molecular weight of 604.48 and a flat molecular area of  $196 \text{ \AA}^2$ . Its structure is shown in the following figure.

A monolayer coverage is assumed for this dye adsorption onto soil surface. The experimental procedures for specific surface area measurement were as follows:



The structure of New coccine dye

- a) Weigh a certain amount of air dried soil (typically 2-3 g/L) into a 1000 mL beaker. Add distilled water to the 1000 mL mark
- b) Adjust the pH of soil sample to 2 by adding  $\text{HClO}_4$  stock solution. Adjust ionic strength if necessary.
- c) Measure the suspended solids (SS) concentration .
- d) Distribute 100 (or 50) mL soil sample to a series of 125 mL plastic bottles.
- e) Add different amounts of stock dye solution into these bottles. The following initial dye concentration are suggested:  $1 \times 10^{-6}$ ,  $2.5 \times 10^{-6}$ ,  $5 \times 10^{-6}$ ,  $7.5 \times 10^{-6}$ ,  $1 \times 10^{-5}$ ,  $1.25 \times 10^{-5}$  M.
- f) Shake the bottles in a shaker for 30 minutes to achieve equilibrium.
- g) Centrifugate each mixture at 15,000 rpm (550g) for 10 minutes to separate the soil from supernatant.
- h) Prepare a series of standard stock solution with known concentrations of coccine dye for the purpose of calibration.
- i) Read and record the absorbance of the standard solutions and the sample supernatant by calorimetric method using a visible spectrophotometer (Hach model DR/2000, Hach Co., Loveland CO) at a wavelength of 505 nm.
- j) Calculate the concentration of the dye remained in samples using the linear regression equation obtained from the calibration curve.
- k) Calculate the maximum dye adsorption density,  $\Gamma_m$  using a multilayer adsorption equation.
- l) Compute the surface area by the following equation:

$$S = \Gamma_m NA$$

where: S is the specific surface area of the soil ( $\text{m}^2/\text{g}$ );

$\Gamma_m$  is the maximum monolayer dye adsorption density (mole/g);  
 $N$  is the Avogadro's number ( $6.023 \times 10^{23}$  molecules/mole);  
 $A$  is the area occupied by a single dye molecule ( $m^2/\text{molecule}$ ).

The multilayer adsorption model developed by Wang and Huang (1997) can be expressed as:

$$\Gamma = \frac{\Gamma_m K_1 C}{(1 - K_2 C)[1 + (K_1 - K_2)C]}$$

where:  $\Gamma$  = overall dye uptake density (mole/g-SS)  
 $\Gamma_m$  = monolayer uptake density (mole/g-SS)  
 $K_1$  = constant related to the adsorption energy for binding to the particle surface ( $M^{-1}$ )  
 $K_2$  = constant related to the adsorption energy for multilayer adsorption ( $M^{-1}$ )  
 From the experimental data of the  $\Gamma$ -  $C$  relationship, the constants  $K_1$ ,  $K_2$ , as well as  $\Gamma_m$  can be obtained by a nonlinear regression method.

### A.7. $pH_{ZPC}$

Take the soil samples from the containers, dry at 105 °C, grind and then sieve through a mesh No. 100 (150  $\mu\text{m}$ ).

For each sample, prepare a solution of 0.1 g/L of the pretreated soil in ionic strength of 0.05 M  $\text{NaClO}_4$ . The zeta potential was measured with a zetameter (Laser Zee model 500) as a function of pH values ranging from 2 to 9. Plot the  $\zeta$  values vs. pH and then the  $pH_{ZPC}$  is obtained at the pH of zero zeta potential

### A.8. Hydraulic Conductivity and Hydraulic Permeability

A constant-head permeameter was used to measure hydraulic conductivities as shown in the below figure. Water entered the medium cylinder from the bottom and was collected as overflow after passing upward through the soils.

From Darcy's law it follows that the hydraulic conductivity can be obtained from:

$$K = \frac{VL}{Ath}$$

where  $V$  = flow volume in time  $t$

$A$ ,  $L$  and  $h$  are shown in figure.

Hydraulic Permeability  $k$  can be calculated by the below equation

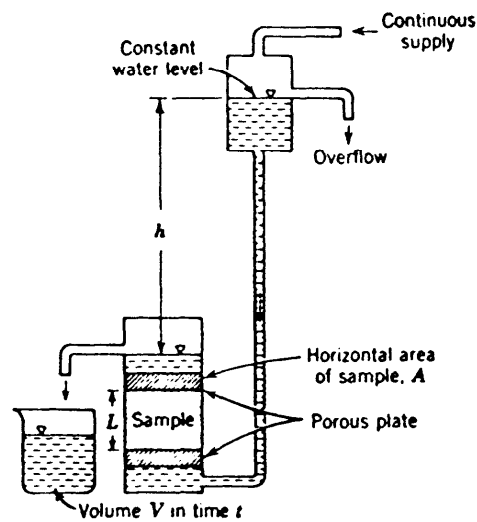
$$k = \frac{K\mu}{\rho g}$$

where  $K$  = hydraulic conductivity

$\mu$  = dynamic viscosity

$\rho$  = the fluid density

$g$  = acceleration of gravity



## A.9. Organic Compounds in Soils

The qualitative analysis of organic compounds in soils is conducted by mixing 2 g soil sample with 2 mL 1N  $H_2SO_4$  and 8 mL hexane in a glass tube. The mixture was shaken for 2 hours. After shaking, centrifuge the mixture at 10,000 rpm for 20 minutes and get the supernatant analyzed by GC/MS.

## A. 10. Heavy Metals in Soils

The experimental procedures for the fractionation of heavy metals in the soil samples were the same as described by Oake et al. (1984) and Rudd et al. (1988). The method consists of using sequential extraction with a series of reagents and dividing the metals present into fractions extracted by potassium nitrate ( $KNO_3$ ), potassium fluoride (KF), sodium pyrophosphate



- |       |           |
|-------|-----------|
| rate  | 0 °C /min |
| final | 100 °C    |
- Carrier gas: 90% argon/10% methane
- Column head pressure 12 psi
- Injection volume: 1 µL
  - Run time: 10 min

All the determinations of the contaminant concentration in the soil were executed in duplicates. Previous studies demonstrated that the extraction method provided recovery efficiencies of more than 90 %. Simultaneously, a calibration curve with known concentrations of the correspondent phenolic compound was prepared and the statistical method of linear regression was used to fit the G.C. signals as a function of concentration and determine the contaminant concentrations in samples.

## **B.2. Contaminant Analysis in Water Solution**

### a). Phenol

Water samples containing phenol were filtered through 0.45 µm membrane filter (Supor-450, Millipore Co., Bedford, MA) and direct analysed using an UV-visible spectrophotometer at wavelength of 271 nm similarly as described previously. Dilutions were performed when necessary.

### b). Mono-Chlorophenols

Liquid extraction and GC-ECD were employed to the analysis of the phenolic compounds in water solution. To 1 mL of the solution containing the target compound, 5 mL of hexane was added. The mixture was shaken for 5 minutes and the organic phase was then ready for the GC-ECD analysis. The GC conditions were the same as described in the previous section. The analysis of the phenolic compounds in water were also done in duplicates using a pre-prepared calibration curve.

## **C. Electra-Fenton Experiments**

### **C.1. Hydrogen Peroxide**

The hydrogen peroxide concentration was measured by a calorimetric method using a Hach DR/2000 direct reading spectrophotometer. The experimental procedures for the hydrogen peroxide measurement were as follows:

- a). Mix 0.504 g titanium sulfate [ $\text{Ti}(\text{SO}_4)_2$ ] and 1.6 g ammonium sulfate [ $(\text{NH}_4)_2\text{SO}_4$ ] in 50 mL concentrated sulfuric acid.
- b). Heat the solution on a hot plate at 100 °C until the titanium salt is completely dissolved.
- c). Dilute the heated solution to 1000 mL with distilled water.
- d). Mix 9 mL titanium reagent with 1 mL aliquot of the sample containing hydrogen peroxide in a test tube.
- e). Heat the test tube in a water bath at a constant temperature (57~63 °C) for 10 minutes.
- f). Cool the sample down back to room temperature before it is analyzed in the spectrophotometer.